AALBORG UNIVERSITET

Det Teknisk-Naturvidenskabelige Fakultet
Aalborg Universitet

Basisuddannelsen

TITEL:
P2 project - Carbon Nanotubes

PROJECT PERIOD:
February 2. - May 30. 2005

PROJECT GROUP:
Nano, A219

GROUP MEMBERS:
Nikolaj L. Kildeby
Ole Z. Andersen
Tom Larsen
Jacob F. Riis
René Petersen
Rasmus E. Røge

SUPERVISORS:
Peter Fojan
Lars Bo Henriksen

NUMBER OF COPIES: 10

NUMBER OF PAGES: 76

NUMBER OF APPENDICES 6

TOTAL NUMBER OF PAGES 98

SYNOPSIS:
This project is based on the initiating problem: "Which problems concerning integration of carbon nanotubes in products exists?" The theory behind characterization of CNTs and their electrical-, mechanical-, optical- and vibrational properties is explained and a description of syntheses techniques and growths mechanisms is made. To describe the electron structure of CNTs a quantum mechanical model is applied.
A solution of HiPCO produced SWNTs in a D_2O 1% SDS solution is used. The solution was sonicated and centrifuged to separate CNT bundles and precipitate aggregates. The techniques absorbance-, fluorescence-, Fourier transform infrared- and Raman spectroscopy is used. Atomic force microscopy and scanning electron microscopy is also used. The techniques are used to determine if the CNTs are separated and to characterize CNTs.
On the theoretical level a description of these techniques are in the related appendices. Considerations about the setup of the equipment are described, and the experiments are discussed.
The conclusion of the report is that the SDS solution can be used to separate the CNT bundles. This is documented by the FTIR and SEM results. Furthermore it is shown that Raman- and absorbance spectroscopy can be used to characterize CNTs. It is also concluded that at the nanoscale it is difficult to get valid data.

Preface

This report is the product of the P2 project period on the basis year of "Aalborg University - Faculty of Engineering and Science", and it has been published by group A219. The purpose of this project is to examine carbon nanotubes as described in the project catalog. The carbon nanotubes used in this project are produced by the HiPCO method. The work that makes the foundation of this report has been going on from February 2th to May 30th, 2005.

The report is for the technically interested reader with a basic knowledge of chemistry and physics, who wants to learn about carbon nanotubes.

The report is build up of an introduction to carbon nanotubes, a problem analysis describing the structure and properties of carbon nanotubes, a method chapter which deals with the scientific method and explains the change of paradigm to quantum physics, a chapter with the materials and methods, a results chapter, a discussion of the results, a conclusion and a perspective chapter. Finally there are different appendices, which describe the techniques thoroughly and technically. There will be references from the report to appendices where appropriate. The experiment data not present in this report can be found on the enclosed CD.

The notation used to references sources is the Harvard method.

We would like to thank Lars Rosgaard Jensen for helping with Raman spectroscopy and Maj-Brit Borksted for helping with electron microscopy.

Contents

Chapter 1

Introduction

1.1 Project description

One of the most famous quotations in nanotechnology is the phrase: "There's Plenty of Room at the Bottom". This quote came from Richard F. Feynman in his famous speech to the American Physical Society in 1959. One of his points in this speech was why no one had been able to write the British Encyclopedia on a pin head. In regard to this Feynman arranged a competition with a price of 1000 dollars, to the person who would first be able to write the British Encyclopedia to a pin head and then read it again. To do this, a new kind of technology, nanotechnology, had to be used, and in 1985 a group of scientists from the Stanford University in USA could collect the award [www.ing.dk, 2005]. This was the first major step in the field of nanotechnology and since then, research and studies has exploded.

One of the main areas in nanotechnology is the possibility to manipulate and make structures on the nanoscale. This can be used to replace or improve the materials used today. One of the new materials originating from nanotechnology is carbon nanotubes (CNTs). Because of their exceptional conductive and mechanical properties, they have been researched and studied thorough since they were discovered in 1991. The properties of CNTs are dependant on several characteristics, such as diameter, length, and chirality. CNTs can be single or multi walled (cylinders nested within other cylinders). Some of the issues regarding CNTs are how to produce and characterize them in such a way, that they can be used to produce new materials and improve existing ones.

1.2 Initiating Problem

As pointed out in the project description there seems to be potential in the use of CNTs in various applications. This leads up to the initiating problem:

- Which problems concerning integration of CNTs in products exists.

Chapter 2

Problem Analysis

2.1 Carbon Nanotubes in a Historic View

The first step in the discovery of SWNT was the identification of the C_{60} structure of carbon by Harry Kroto and Richard Smalley. Kroto was fascinated by the processes occuring on the surfaces of stars and Smalley's main work was in synthesizing clusters mainly of silicon and gallium arsenide, but he also had an interest in vaporization of carbon. These interests brought them together at Rice University in 1985 in a series of experiments leading to the discovery of the C_{60} molecule, also called the buckyball. Using laser vaporization of graphite in a helium atmosphere they produced a carbon soot which they analyzed using mass spectrometry. They detected a large amount of molecules containing 60 carbon-atoms but it was not until they realized the possibility of this structure being a closed sphere, of unique stability and symmetry, they realized the significance of the discovery. More information about the structure and nature of the buckyball can be found in Section 2.2.

Harry and Smalley's work was published in an article in Nature in November 1985 [Harris, 1999]. The next step was to discover a way of producing the C_{60} structures in larger scale and not minuscule as was the case at Rice University. This was accomplished by a process far more simple than the one used in the experiment of Kroto and Smalley at Rice University. Wolfgang Krätschmer and Donald Huffman used a simple carbon arc to vaporize graphite and it was possible to produce crystallized fullerenes by dispersing the soot in benzene and precipitating the fullerenes of the solution. This was published in their article in Nature in 1990 showing macroscopic amounts of fullerenes, stimulating a boost in research. CNTs is one of the fruits of the increased research of buckyballs. [Harris, 1999]

Sumio Iijiama is credited the discovery of CNTs. Inspired by the Krätschmer and Huffman article in Nature and from previously discovered novel nano structures in the soot produced by a similar arc evaporation process, he decided to investigate the soot using TEM microscopy. At first he focused on the wall soot and disappointingly found mainly amorphous structure and not the novel structures he was looking for.

This turned his attention elsewhere and he began studying the hard cylindrical deposit formed on the graphite cathode. Here he found a variety of novel carbon structures including the multiwalled carbon nanotube (MWNT). This was published in an article in Nature in November 1991.

In 1993 two groups independently discovered the single walled nanotube (SWNT). Sumio Iijiama and Toshinari Ichihashi of NEC, and Donald Bethune and colleagues of the IBM Almaden Research Center in California was responsible for this discovery. The SWNT has proven to resemble the ideal nanotube both in structure and in properties. The focus of this report will be placed on SWNTs.

2.2 Buckyball

Buckyballs are a group of carbon molecules consisting of 20 to 500 carbon atoms arranged in a hollow sphere. The carbon atoms are organized in pentagons and hexagons. All buckyballs contain 12 pentagons and a number of hexagons, which depend on the amount of carbon atoms. As mentioned in the previous section C_{60} was the first discovered buckyball. The molecule was named after the American architect R. Buckminster Fuller, whose geodesic dome is constructed on the same structural principles. A C_{60} molecule contain the required 12 pentagons and furthermore 20 hexagons. This structure is similar to the pattern of a soccer ball. The C_{60} molecule contain the best properties of diamond and graphite, and it have inherited the high stability of diamond and the excellent conducting abilities from graphite. Figure 2.1 is an illustration of the C_{60} buckyball. [www.britannica.com, 2005]

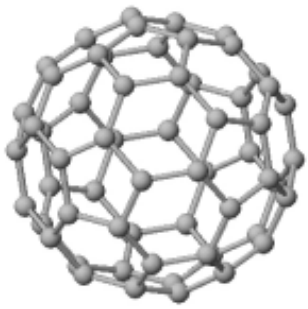

Figure 2.1: The first discovered C_{60} buckyball. [www.britannica.com, 2005]

2.3 Characterization

CNTs are cylinder formed carbon structures with a diameter of approximately $1nm$ and a length of approximately 100 μm [Jr. and Owens, 2004]. This property makes them effectively a one dimensional structure. The CNTs are formed by carbon atoms placed in hexagonal rings like aromatic structures, composing a flat graphene sheet that looks like honeycombs. The sheet is rolled up to form a tube. In the end of the

tubes a round-shaped carbon structure, such as the Buckyball, can be used to close the tube. This is however not always the case as the tubes can be open ended. CNTs can either be single walled, or nested inside each other. If only one individual tube is present, it is called a single walled carbon CNT (SWNT), and if two or more tubes are nested inside each other, they are called multi walled carbon CNTs (MWNT).

Theoretical studies of CNTs indicate the importance of the surface structure to the electrical properties (see Section 2.4 for more information on the electrical properties). Thus, a system of naming different types of surface structure is needed. This is done using two vectors: The vector $\mathbf{C_h}$ and the translational vector $\mathbf{T}$.

The vector $\mathbf{C_h}$ expresses the circumference and is defined by two integers n and m, $\mathbf{C_h} = n\mathbf{a_1} + m\mathbf{a_2}$. It is best visualized through a single layer of graphene as a two dimensional honeycomb lattice. The vectors $\mathbf{a_1}$ and $\mathbf{a_2}$ are the primitive vectors of the lattice, see Figure 2.2. The translational vector $\mathbf{T}$ is perpendicular to $\mathbf{C}_h$ and directs the length axis. The length of the translational vector is given by the first encounter of a lattice point yielding the length of the unit cell of the CNT. By these two vectors both the circumference and the orientation of the CNT on the honeycomb lattice are given. This entails that different types of CNTs can be given by the set of integers (n, m).

The diameter of a CNT can be derived from the (C_h, a_1, a_2) triangle yielding Equation 2.1.

$$d_t = \frac{|C_h|}{\pi} = \frac{\sqrt{3}a_{c-c}\sqrt{n^2 + m^2 + nm}}{\pi} \tag{2.1}$$

a_{c-c} is the length of the C-C bonds and is equal to $1.44\mathring{A}$ in CNTs. The angle θ can be limited between zero and thirty degrees due to symmetrical reasons thereby limiting the integers n and m from $(n, 0)$ to (n, n). $(n, 0)$ corresponds to $0°$ and is called zig-zag CNTs. Between $0°$ and $30°$ the structure is chiral. (n, n) integers correspond to $30°$ and the structure is called armchair. See Figure 2.3 for examples. The example shown in Figure 2.2 is a $C_h = (4, 2)$ CNT with $T = (4, -5)$ and $d_t = 4.2\mathring{A}$.

In Figure 2.4 the different $\mathbf{C_h}$ vectors and their respective pair of (n, m) integers are shown. Their conducting properties are indicated by the black dots. Note that the honeycomb lattice is rotated compared to Figure 2.2.

The SWNT produced today is a mixture of zig-zag, armchair and chiral CNTs. Therefore, the measured properties are average values of the bulk CNTs and not for the individual CNTs. Today it is not possible to control the production rate of each type of CNT. Nor is it possible to seperate one type from the other. This is something which is needed in the future, in order to fully take advantage of the electrical properties of SWNT. [Dresselhaus et al., 2001]

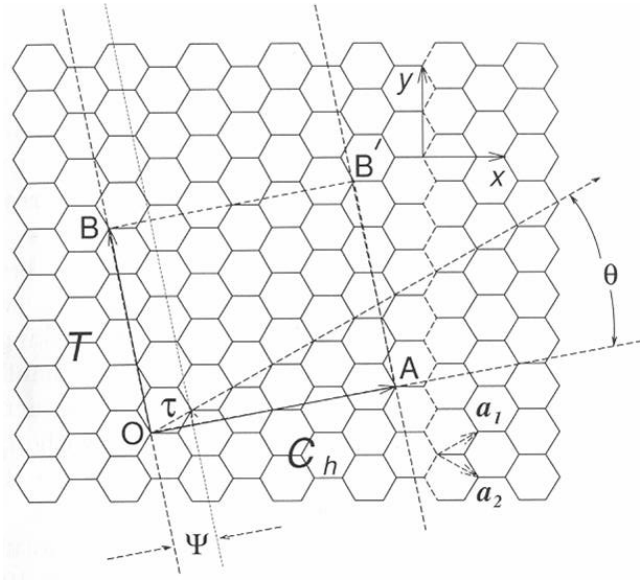

Figure 2.2: The Translational vector, $\mathbf{T}$ *and the* C_h *vector is shown for the* $(n, m) = (4, 2)$ *CNT on the honeylattice. [Dresselhaus et al., 2001]*

2.4 Structure and Properties

Due to their highly interesting characteristics CNTs are today one of the most examined structures on the nano scale. They combine properties such as high strength in spite of a low stiffness, and the ability to conduct electricity with low resistance. This section will describe the electrical, mechanical, optical and vibrational properties of CNTs.

Electrical properties

One of the most interesting aspects of CNTs are their electrical properties. The CNTs can be either metallic or semiconducting with different size band gaps. As described in Section 2.3 these electrical properties depend on the geometric structure such as the diameter and chirality. The chirality is defined by the set of integers (n, m) as described in Section 2.3. In general, the armchair tubes, also called (n, n) tubes, are metallic, while (n, m) tubes with $n - m = 3j$, where j is a nonzero whole number, are tiny-gap semiconductors. All others are large-gap semiconductors. $(1, 1)$ and $(4, 4)$ tubes, for instance, are metallic, and $(3, 0)$ and $(7, 1)$ tubes are small-gap semiconductors while $(5, 0)$ and $(3, 1)$ tubes are large-gap semiconductors. [Dresselhaus et al., 2001]

The $n - m = 3j$ tubes would all be metals strictly within the band-folding scheme, but because of tube curvature effects a tiny gap opens. At room temperature however, the variety in gap caused by the curvature effects would be so small that the $n - m = 3j$ tubes are considered metals for practical reasons. This means that

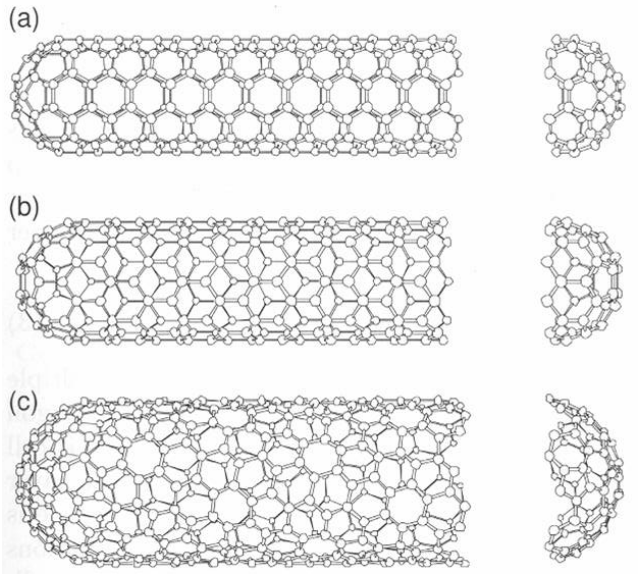

Figure 2.3: Here examples of (a) armchair (5,5), (b) zig-zag (9,0) and (c) chiral (10,5) CNTs respectively are figured.
[Dresselhaus et al., 2001]

the $(3, 0)$ and $(7, 1)$ tubes would be metallic. This is also illustrated on Figure 2.4. An explanation of band gaps can be found in Section 2.12. The armchair structure is independent of these curvature effects because of it's symmetry. Therefore the electrical properties can be described with three variations: large-gap, tiny-gap and zero-gap. [Dresselhaus et al., 2001]

For tubes with diameters above 1 nm it applies that the large and tiny gaps are dependent on the radius R. As R increases, the large-gap and tiny-gap decreases with a $1/R$ and $1/R^2$ dependence respectively. This dependency does not apply to tubes with diameters below 1 nm where strong rehybridization among the σ and π states can alter the electronic structure of the tubes due to the curvature effect. The energy gaps for small tubes are decreased by more than 50%. This means that the $(6, 0)$ tubes which should be semiconducting actually proves to be metallic as shown in Figure 2.4. [Dresselhaus et al., 2001]

Mechanical properties

CNTs are one of the strongest molecules known. The main reason for this is the low appearance of defects in the structure, allowing the tubes to bend and to straighten back and forth with low probability of breaking. However, as a consequence of the fact that a CNT can occur both as a crystal and as a molecule, the traditional measuring methods show up to be insufficient and unreliable. The standard starting point for measuring the elasticity modulus C is shown in Equation 2.2.

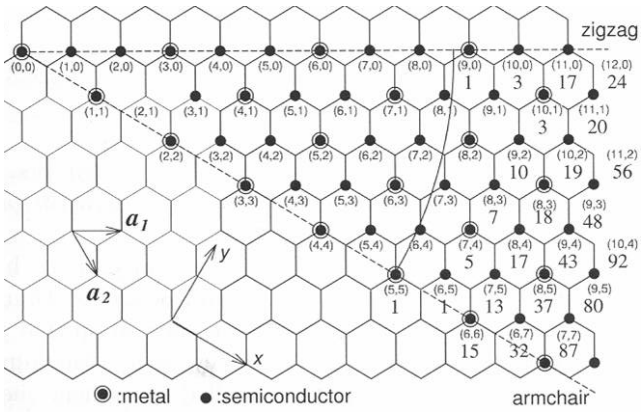

Figure 2.4: This illustrates some of the possible vectors in a CNT specified by the integers (n, m). It shows the armchair structure to be metallic, while the zigzag and chiral structure are around $1/3$ metallic and $2/3$ semiconducting, illustrated by the encircled dots and dots, respectively. [Dresselhaus et al., 2001]

$$C = \left(\frac{1}{V}\right)\left(\frac{\partial^2 E}{\partial \varepsilon^2}\right) \tag{2.2}$$

Where the total energy E is a function of uniform strain ε only works for CNTs, if the strain is in the axial direction. Any other deformation induces non-uniform strain, which yields this expression misleading. Also, the volume V is not well defined for a hollow CNT, as the cross sectional area A can be measured in several arbitrary ways, making the volume V and thus the modulus ambiguous. This uncertainty is best eliminated by considering the internal energy in the CNT per area S of the graphite layer instead of the volume. The two dimensional structure of the graphite layer ensures that the area is well defined; hence the modulus C can be defined as:

$$C = \frac{\left(\frac{1}{L}\right) \cdot \left(\frac{\partial^2 E}{\partial \varepsilon^2}\right)}{\int dl} \tag{2.3}$$

Where L is the length of the CNT, and l is the total circumferential length of the graphitic layers in the cross section of the CNT. This expression corresponds to Young's modulus Y when no lateral traction in the CNT is present, so that Y can be expressed as:

$$Y = C \cdot \int \frac{dl}{A} \tag{2.4}$$

Young's modulus is a measure of the elasticity in length of a material, and is defined as the resistance of a solid to a change in its length, which can be expressed as:

$$Y = \frac{stress}{strain} = \frac{\frac{F}{A}}{\frac{\Delta L}{L_i}} \tag{2.5}$$

Where ΔL is the change in length, L_i is the original length, F is the external force and A is the cross-sectional area of the material [Serway and Jewett, 2004]. Many different methods have been used to measure the Young's modulus for CNTs, which is a rather challenging task. For obvious reasons, traditional methods can not be used.

One experiment has correlated the amplitude of the thermal vibrations of the free ends of anchored CNTs as a function of temperature with the Young's modulus. This technique measured Young's modulus to be around 1.8 TPa on average, but with the significant scatter in the data, as the result varied from 0.4 to 4.15 TPa for individual tubes. Another experiment used an AFM tip to bend anchored CNTs while measuring the force exerted by the tube as a function of its displacement. This test gave a Young's modulus at 1.28 $\pm$ 0.5 TPa. An interesting observation in this test was that the Young's modulus showed no dependence of the diameter of the tubes [Dresselhaus et al., 2001]. Other methods have also measured Young's modulus to be 1.28 to 1.8 TPa. This is a high result compared to other known substances, for example steel, which has a Young's modulus at 0.2 TPa and aluminium at 0.07 TPa [Serway and Jewett, 2004]. This indicates that CNTs indeed are strong, and it also indicates that they are hard to bend. The latter is however not quite true because of the low wall thickness. [Jr. and Owens, 2004].

The tensile strength of a material is a measure of the amount of stress needed to pull the material apart. For SWNT the strength have been calculated to be about 45 GPa, which is more than 20 times the strength of steel. [Jr. and Owens, 2004]

Vibrational properties

In a lattice all atoms undergo fluctuations from their surroundings such as heat or thermal energy. These fluctuations exist even at zero Kelvin but become more distinct at higher temperatures. As chemical bonds bind atoms together, the movement from one atom affects another and causes this to respond to the movement. A chemical bond acts like a spring, meaning that it stretches and compresses. When many atoms vibrate simultaneously their collective obtained motion spreads throughout the crystal. Each type of lattice has a characteristic frequency of vibrations [Jr. and Owens, 2004]. From the vibrations of the molecules in the CNT solution it can be determined which molecular bonds the substance contains. This can be done using Fourier Transform Infrared Spectroscopy. This method is described in details in Appendix C.

The vibrations in CNTs have the special property that a measure of the vibrational frequency can be used to measure the radius of the tube. This is possible because the frequencies are Raman-active and are dependant on the radius of the tube. CNTs vibrate in different ways. One of them, labeled E_{2g}, squashes the tube. This means that it squeezes down in one direction and expands in the perpendicular

direction essentially oscillating between a circle and an ellipse. Another mode, the A_{1g} mode, involves an in-and-out oscillation of the tube diameter. This mode is also known as radial breathing mode or RBM [Jr. and Owens, 2004]. Figure 2.5 illustrates the RBM of the CNTs. Another vibrational mode is the tangential mode or G-band. This mode is illustrated in Figure 2.5 [Dresselhaus et al., 2002].

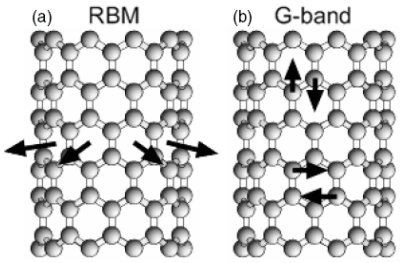

Figure 2.5: The figure illustrates (a) The motion of the atoms in the vibration mode of the RBM. (b) The motion of the atoms in the G-band vibration mode of the CNTs [Dresselhaus et al., 2002]

Optical properties

When light interacts with the aromatic system of the CNTs, absorption and emission of photons takes place. At which wavelengths these phenomena appears depends on the diameter of the CNTs. The diameter of CNTs is proportional to the wavelength at which it absorbs and emits light. Absorption can appear without resulting emission. If the (n, m) integers can be controlled to perfection, a single diameter can be produced and this can be utilized to produce fiber optical wires with CNTs.

The interaction between light and CNTs can be monitored at different wavelengths using absorbance- and fluorescence spectroscopy. These methods are described in Section 4.2. The data from these two methods can be used to calculate the different (n, m) assignment of the CNTs present in the solution. [Bachilo et al., 2002]

2.5 Synthesis of CNTs

The potential of CNTs is indeed huge, but the full potential will not be revealed before the growth of CNTs can be optimized and well controlled. Today four methods have been developed in order to grow SWNT and MWNT, but a complete protocol for CNT growth have not yet been developed. A hotchpotch of problems are linked with the production of CNTs. The primary problems are insufficient control of the structural properties, low purity of the produced CNTs, and too high production

prices. To solve these problems more research in this area is needed. This section will give a description of the methods.

Chemical Vapor Deposition

Chemical Vapor Deposition, or CVD for short, refers to the process of depositing a gas on a surface without the gas first being condensed and liquidized. This makes deposition the opposite process of sublimation in which a solid undergoes a phase change from solid to gas, again, without first liquidizing. CVD has been widely used in integrated circuit (IC) manufacturing. In IC manufacturing a thin film of silicon is deposited on a support substrate by CVD, to create a semiconduction thin film layer. For CNT growth by CVD a somewhat different method is used, but it is still called CVD though. Where a catalyst is almost never used for CVD manufacturing of IC devices, CVD manufacturing of CNT always requires a catalyst [Goddard, 2003]. CVD is becoming the preferred method of CNT production because of the relatively low temperatures needed for production. Arc-discharge for example relies on temperatures ($> 3000°C$), which is not efficient. [Dresselhaus et al., 2001]

The setup of CVD for CNT growth is pretty simple. Basically it consists of a quartz tube enclosed in a furnace. The quartz tube is typically $5 - 10cm$ in length and capable of holding small substrates. The substrate being held is a support substrate prepared with the catalyst. Often the support substrate is chosen to be alumina [Dresselhaus et al., 2001]. Alumina is chosen for the nanosized pores found in its surface. The pores in alumina are filled with catalyst increasing the surface area and thereby the yield of CNTs. After the preparation the furnace is heated to $500 - 1000°C$. Which temperature is chosen depends on the type of CNTs to be produced. For MWNT growth a temperature of $550 - 750$°C is often used, and for SWNT $850 - 1000$°C is used [Dresselhaus et al., 2001]. After heating the furnace, a hydrocarbon gas is being flowed through the quartz tube. The light hydrocarbons like methane and ethane is chosen due to their stability against self decomposition at high temperatures. This makes the decomposition of the hydrocarbon by the catalyst the dominant process [Dresselhaus et al., 2001]. When the carbon feedstock is decomposed by the catalyst it is dissolved in the metal particles. This causes a saturation and therefore a precipitation. The precipitation of carbon from the saturated metal particles, causes the formation of tubular graphitic sheets or CNTs. The formation of tubular sheets is preferred over plain graphitic sheets with open ends. The open ends of graphitic sheets contain dangling bonds whereas the tubular sheets contain no or fewer dangling bonds and is therefore energetically favorable. An schematic setup of the CVD method described is shown in Figure 2.6.

Among the methods used for CNT growth, CVD has shown to be the most promising due to the high yield of nearly defect free CNTs and the possibilities of scale-up of production. CVD is likely to be the preferred method of CNT growth in the future.

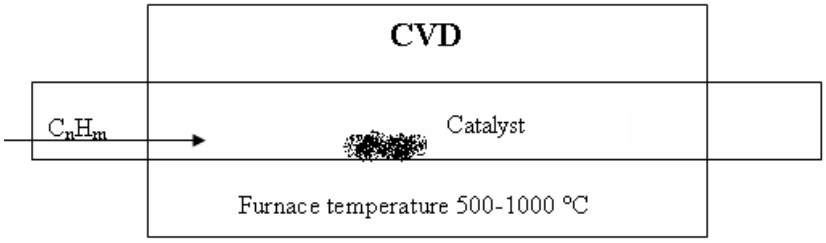

Figure 2.6: A schematic setup for the CVD system.

High Pressure Carbon Monoxide

SWNT can be produced by the high pressure carbon monoxide method (HiPCO). In this method carbon monoxide is used as the feedstock and iron pentacarbonyl ($Fe(CO)_5$) as the carrier of the catalyst. The setup of HiPCO is illustrated in Figure 2.7. The two gases are lead into a furnace through a water cooled injector at a constant flow of $1 - 10$ atm. The water cooled injector keeps the temperature of the gases down until they enter the center of the furnace, where the temperature is between 800 and 1200°C. When the two gases enter the hot center, $Fe(CO)_5$ produce iron clusters in gas phase created by the thermal decomposition. These clusters act as a nucleus upon which the SWNTs starts to grow. The solid carbon is formed by the Boudouard reaction:

$$CO_{(g)} + CO_{(g)} \rightarrow C_{(s)} + CO_{2(g)} \tag{2.6}$$

It has experimentally been proved that the process can be optimized by adding an amount of preheated CO gas to the center of the furnace [Nikolaev et al., 2004]. A HiPCO production yields a high amount of CNTs and the diameter of the SWNT can vary from $0.7 - 2.4$nm but the width of the diameter distribution is not very reproducible resulting in an indeterminate distribution. These SWNTs are almost perfect and without pollution in the form of fullerenes, amorphous carbon and graphite. Because of these qualities the HiPCO method is apposite for scale up of production of SWNTs [Nikolaev et al., 2004].

Laser Ablation

Another method to produce SWNT is laser ablation. This method utilizes an intense laser to ablate a carbon target containing nickel or cobalt as catalyst. Figure 2.8 illustrates the setup for this method. The target is placed inside a furnace, which retain a temperature of 1200°C. During the ablation an inert gas such as helium or argon is flown through the furnace. The gas carry the carbon atoms though the furnace and towards a water-cooled copper collector where the atoms condense into CNTs [Dresselhaus et al., 2001]. Laser ablation can also be used to produce MWNT. The setup is the same, except of the target, which in this case

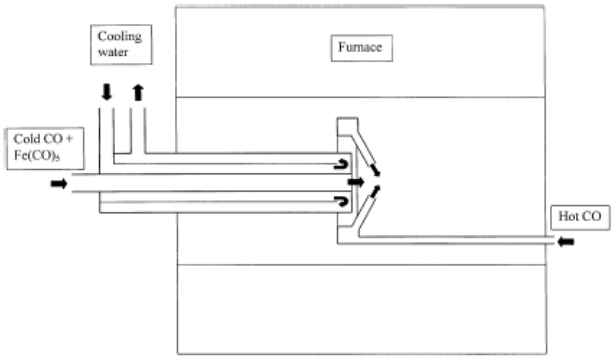

Figure 2.7: A setup for the HiPCO system [Nikolaev et al., 2004]

does not contain any catalyst [Harris, 1999]. The produced CNTs have almost perfect sidewalls but they are polluted with graphite, fullerenes and amorphous carbon. The diameter of the produced CNTs is similar to those achieved with arc-discharge [Dresselhaus et al., 2001].

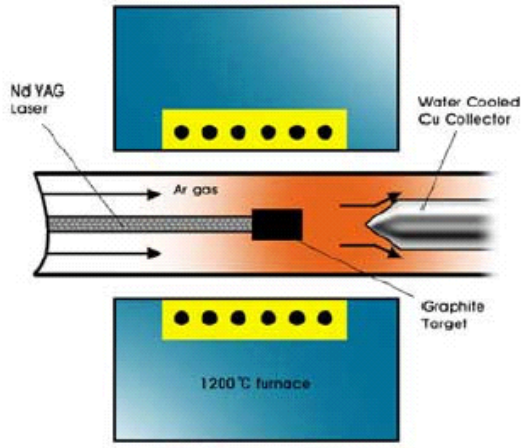

Figure 2.8: A schematic picture of the laser ablation setup [www.iljinnanotech.co.kr, 2005]

Arc-Discharge

Arc-discharge was the method that Iijima used to produce fullerenes in 1991, when he discovered that CNTs were a by-product from this method. Since 1991 arc-discharge has been developed into a method that can produce both MWNT and SWNT [Harris, 1999]. In arc-discharge a potential of 20-25 V is applied across two

$1mm$ separated carbon electrodes of 5-20 μm in diameter, and a helium gas at 500 torr pressure is flown through the system, see Figure 2.9. Carbon atoms are thereby ejected from the positive electrode and form CNTs on the negative electrode. The temperature where this process takes place is close to the melting temperature of graphite, which lies between 3000 and 4000°C [Dresselhaus et al., 2001]. MWNT can be obtained by controlling the growth parameters under the production, such as the pressure of the helium gas and the arcing current. Through this method it is today possible to synthesize MWNTs, which are more than ten micrometers in length, has an inner diameter of $1 - 3nm$ and an outer diameter of approximately $10nm$. For producing SWNT with an arc-discharge system it is necessary to add a metallic catalyst. Nickel, iron, cobalt or yttrium can be used as catalyst and it is placed inside the carbon anode. The remaining setup is the same as in the production of MWNT. The diameter of the SWNT lies between $1.2nm$ and $1.4nm$ [Dresselhaus et al., 2001]. The arc-discharge method produces CNTs with few defects on the sidewalls of the CNTs. A by-product of the arc-discharge is multi layered graphitic particles, fullerenes and amorphous carbon. [Dresselhaus et al., 2001]

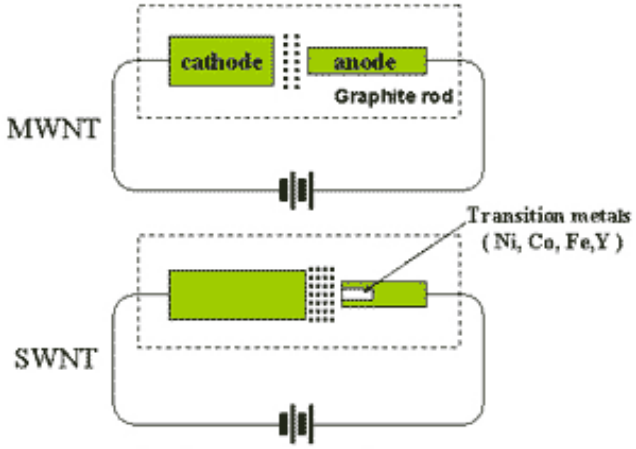

Figure 2.9: A schematic diagram of the arc-discharge apparatus [www.iljinnanotech.co.kr, 2005]

2.6 Growth Mechanisms

Today there is no method of synthesis available for large scale production of CNTs. The methods are limited by high temperatures and relatively slow reaction processes. Large scale production is however important for the integration of CNTs in industrial products. The current methods of synthesis have been developed on the basis of a few experimental facts, such as the need for a catalyst and enough energy to free carbon atoms from the reagents.

The surface of the CNTs are made of hexagons and pentagons. Six pentagons are used for closure of the CNTs while the wall of a perfect CNT consists of only

hexagons. If pentagons or heptagons are added in the wall of a CNT it results in a deviation from the straight structure in the form of turns or twists. A pentagon will result in a positive curvature (convex) and a heptagon will result in negative curvature (concave). See Figure 2.10 for examples. [Dresselhaus et al., 2001]

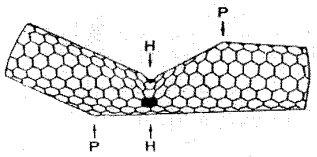

Figure 2.10: The result of adding a heptagon or a pentagon. [Dresselhaus et al., 2001]

Controlling the shape of a CNT through the addition of pentagons and heptagons could be an important step in the use of SWNT, although it lies distant in the future. Through this it could become possible to control the size and shape of the SWNT.

The need for Catalysts

One of the main differences between production of SWNTs and MWNTs lies in the need for a catalyst. This indicates a different growth mechanism between the two. Calculations have indicated that CNTs of diameter smaller than $3nm$ would lead to spontaneously closure if carbon is added resulting in the formation of fullerenes. Calculations have also shown that CNTs of small diameters could close spontaneously at production temperatures between $2000K$ and $3000K$. This indicates the need for catalysts in the formation of SWNTs and therefore the key to understanding the formation of CNTs must lie in the precise role played by the catalyst. [Dresselhaus et al., 2001]

Scooter Model

In the scooter model an initiating fullerene is formed with Co or Ni atoms sitting at the open end. The diameter of the fullerene will determine the diameter of the SWNT. The diameter is set as the optimal value with respect to strain energy due to curvature on one side and the dangling bond energy of the open edge on the other.

Calculations indicates that the Co or Ni atoms, though strongly bound, are still very mobile at the growing edge. This indicates that the Co or Ni atoms are scooting around the edge of the CNT inhibiting the formation of closing pentagons.

Locally the catalytic atom is assisting the formation of hexagons and thereby catalyzing the continuous growth. However, the catalyzing effect requires single atoms and as the concentration of metal atoms is constant several atoms will aggregate. This will stop the catalyzing effect and pentagons will form and close the tube end. This aggregation will also decrease the adsorption energy of the metal cluster causing the particle to reach a critical size and "peel off". One indicating factor in this model is that no observable metal particle is left at the tube ends. This is illustrated in Figure 2.11. [Dresselhaus et al., 2001]

First principle molecular dynamics calculations of a simulation at $1500K$ have however indicated continuous closed-end growth. The metallic atom is incorporated in the CNT cap in a frequently breaking cobalt-carbon chemical bond. In this model a similar principle of closing could be applied as multiple metallic atoms are incorporated and thereby loosing the catalytic effect and adsorption energy. This closed-end growth is also illustrated in Figure 2.11.

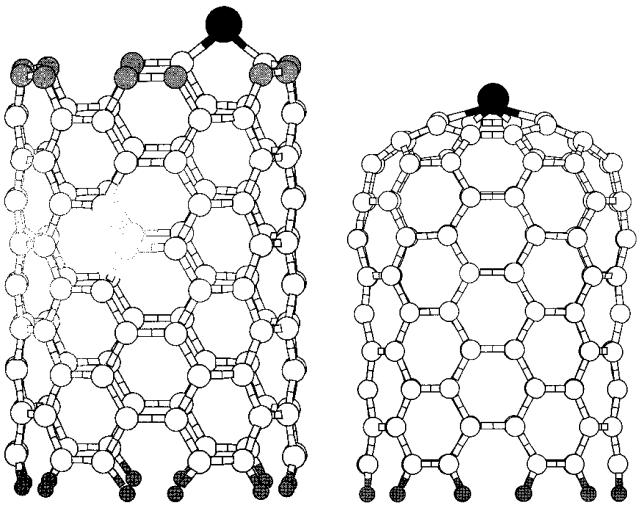

Figure 2.11: To the left the scooter model is illustrated. The metallic catalyst is strongly bound though very mobile at the end of the CNT resulting in a scooting effect that prevents the formation of pentagons. To the right the closed-end growth is illustrated. The tube as the Cobalt-Carbon bond is breaking and reforming carbon atoms are incorporated into the CNT. Modified from [Dresselhaus et al., 2001]

Metal Covered Fullerenes as a Catalyst

Another model of the catalytic effect is the catalytic metal surface decorated fullerene. A fullerene adsorbing Ni or Co atoms in order to decorate the surface with the catalytic metals could trigger the growth of a SWNT by acting as a template. The decorated fullerene would act as the template for the CNT and trigger growth. Once started the particle would not be necessary. Although the complicated appearance of this model the calculated average diameter, the sum of the diameter of the fullerene added two times the metal ring distance $(0.7 + 2 \cdot (0.32 \pm 3)nm \approx 1.4nm)$ is in consistency with the measured average value, 1.4nm. [Dresselhaus et al., 2001]

Vapor-Liquid-Solid

Another way of looking at the catalytic particle at the tip of the CNT is through the vapor-liquid-solid (VLS) model. The VLS model has its name from growing silicon whiskers. Vapor silicon is added to a tiny catalytic droplet at the tip of

the filament. Silicon then precipitates from the supersatuated droplet resulting in formation of faceted cylinders or tubular structures. [Dresselhaus et al., 2001]

Regarding SWNT this droplet is reduced to only a few atoms, that however retain the catalytic effect. It is no longer fluid but the chemical reaction between Cobalt 3d electrons and the π carbon electrons enables the rapid incorporation of carbon atoms.

The question of whether to find a small catalytic particle with the size of a few atoms at the tip of the CNT or not is easily answered experimentally. The catalytic remains has yet to be detected although the experiments cannot safely say that there is none. However in some cases multiple CNTs are found with one side embedded in large particles. These observations have led to the root growth model. [Dresselhaus et al., 2001]

Root Growth

During arc discharge metal and carbon particles can condense and form alloy particles that when cooled will result in formation of soot particles approximately 10nm wide. These soot particles will consist of embedded metal particles surrounded by some graphite layers. In some singularities at the surface structure the nuclei for CNTs can form growing mainly by a carbon supply from the graphite layers. An addition of carbon atoms at the tip is also presumed to be aiding the CNT growth. [Dresselhaus et al., 2001]

This hypothesis is supported by the fact that many SWNTs are observed to be connected or with one side embedded in the catalytic particle. The catalytic particle is often found many times larger than the diameter of the CNT.

Neither of these models give a complete description of the catalyst role in the formation of SWNT. However the continuous interplay between experiments and theoretical calculations continue to make improvements enhancing the insight in these processes. The primary aim of these studies is to determine the optimal conditions for the formation of well-designed SWNT making large scale production possible.

A more distant goal could be to control the addition of pentagons and heptagons to the CNT making it possible to control the shape of the CNT. [Dresselhaus et al., 2001]

2.7 CNT Bundles

Under the production of the CNTs, bundles are formed during the condensation part of the process. The bundles are formed when the CNTs stick together due to van der Waals forces. The reason for the strong van der Waals bonding, is that the tubes lie parallel to each other. This orientation means that the surface of contact is maximized, thereby enhancing the strength of the bundle formation. The size of a bundle is determined by the number and size of those the CNTs interacting with

each other. The bundle formation is what makes the raw CNTs visible to the naked eye. [Dresselhaus et al., 2001]

2.8 Applications of CNTs

Carbon bonds are know to be strong, and the two well-known phases of solid carbon, diamond and graphite have been used widely in many applications. The transformation of iron into steel by addition of carbon, to make cutting tools and for creation of high performance polymer composites for use in the aircraft industry, are just examples of the many different uses of the traditionally known carbon structures.

The discovery of the fullerenes, and especially the CNTs, did however show that structures build by sp^2 bonds with simple geometrical principles, results in new structures that have fascinating and, more important, useful properties. Because of the high rate of flawlessness, the structure of the tubes can be fully documented and presented from a unit cell picture. This gives the material a molecular characteristic, allowing scientists to predict the properties of the tubes theoretically, and encouraging experimentalists to predict and find various possible uses for the CNTs. [Dresselhaus et al., 2001]

One should be aware that the following examples of different applications of CNTs all are predictions and visions, and therefore the extent of realization depends on different challenges that have to be coped with first. For example the price of SWNTs still exceeds 200$ per gram [Jr. and Owens, 2004], and the amount of high purity CNTs that can be produced is still very low. This makes the tubes too expensive for industrial use. Due to these reasons further investigation and research of CNTs are essential for the development of industrial products utilizing CNTs.

In certain cases not all properties of CNTs are needed, and the production method can be modified accordingly. If for example the strength is wanted for a composite material, then the purity, and to a certain extend also the separation, of the CNTs is irrelevant. If on the other hand the CNTs are wanted for their optical properties then both the purity and the separation are of great relevance.

Nanoprobes and Sensors

The well-defined dimensions, the electrical and thermal conductivity and the mechanical strength and flexibility, make CNTs perfectly suitable for various forms of probes and sensors. For example applications such as high-resolution imaging, nanoelectrodes and field-emitters make use of CNT probes. Because of the size and strength of CNTs, they can be attached to the tip of a scanning tunneling microscope or atomic force microscope. This improves the resolution of the images, because the CNTs are thinner than the normally used silicon or metal tips. In addition to this, CNTs are very strong which minimizes the chance of breaking the tip.

However, the process of attaching a CNT at the end of an AFM tip is not an easy task. Typically bundles of CNTs are pasted on the tips and the ends are cleaved to

expose individual CNTs. Attempts to grow CNTs directly on silicon tips using the chemical vapor deposition method have been successful.

CNTs attached to AFM tips have shown more remarkable features. For example, pairs of CNTs positioned properly on the tip can be used like tweezers to pick up and release nanoscale structures. Nanolithography is another possible use; writing text on oxidized silicon substrates using CNT tips at high speeds has been accomplished.

Field emission

Field emission is when electrons are emitted at high rate from the ends of the tube. By applying an electric field parallel to the CNTs the emission is observed. This property is being used by different electronic companies for development of high-technology equipment. At Samsung a flat-panel display using this feature is under development. The flat-panel display is made by placing a thin film of CNTs on top of control electronics with a phosphor-coated glass plate on top. Also, the conductivity of the CNTs can be used as shielding against electromagnetic radiation, an attribute that is currently being utilized by the US army. A plastic composite of CNTs is under development, and is intended for the use of protection of computers and other electronic devices, as the CNTs are poor transmitters of electromagnetic energy. [Jr. and Owens, 2004]

Batteries and Fuel Cells

Using CNTs as storage for lithium and hydrogen for use in battery technology and fuel cells respectively, is another possible application. Lithium is the charge carrier in most cell phone batteries, and it is estimated that one lithium atom can be stored for every six carbon atom in CNTs. Storing hydrogen in CNTs is a probable method for storage of the hydrogen atoms used in fuel cells, a potential future energy source for automobiles.

A fuel cell consists of two electrodes separated by an electrolyte that disconnects hydrogen ions from its atoms, allowing only the hydrogen ions to pass through from the anode to the cathode. The electrons are sent through an external circuit wire to the cathode, where it combines with oxygen and hydrogen ions and form water by which energy is released.

The fuel cells need a hydrogen source, and this source could be CNTs with hydrogen stored within it. But first a suitable method of storing hydrogen within a CNT has to be found. One promising method for this is shown in Figure 2.12. Two electrodes, of which the cathode consists of CNTs and the anode consists of $Ni(OH)_2$, are placed in a $6MKOH$ water solution. The water in the electrolyte solution is decomposed into positive hydrogen ions which are bonded to the negative CNTs. [Jr. and Owens, 2004]

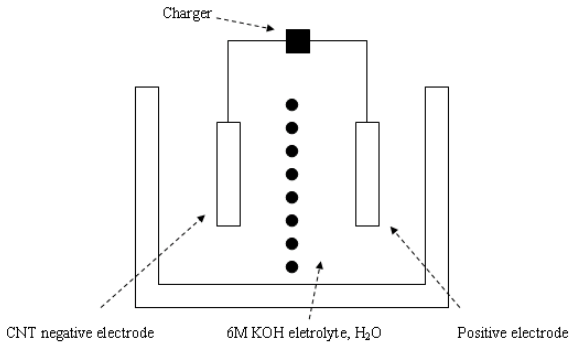

Figure 2.12: A model for an electrochemical cell used to inject hydrogen in CNTs. The cell consist of an electrolytic solution of KOH with a negative and positive electrode. The negative electrode consist of CNT paper. Voltage between the electrodes causes the H^+ ion to be attracted to the negative electrode.

Mechanical Reinforcements

Incorporating CNTs in aluminium is one example of improving the tensile strength of materials. At an experiment in Tokyo aluminium powder at 5% vol. CNTs, is heated to over $800K$ and mixed in vacuum. Thereafter the mixture is compressed with steel dies and extruded into rods. These rods appeared to be twice as strong as normal aluminium rods, and theoretical estimations suggests that the strength could be optimized by a factor 6 with proper operations. [Jr. and Owens, 2004]

The challenges to be solved before CNTs can be used in structural reinforcements are the ability to create a good interface between the CNTs and the polymer matrix, and ensuring a good load transfer from the matrix to the CNT. The major problem is to prevent the sliding between individual layers in CNT, and the sliding of individual CNT in ropes. This indicates that CNT ropes will have to be dispersed or cross-linked internally, so that the sliding does not occur.

Sliding between the CNTs in ropes can be avoided if the length of the CNTs is big enough. In 2003 scientists at the University of Texas at Dallas proved that strong pure CNT fibres can be made. The scientists produced fibres made from pure single walled CNTs. These fibres proved to be up to 4 times stronger than spider silk, which is one of the strongest known materials. The individual CNTs within the fibres are held together by the intermolecular forces present within CNT bundles. The longer the CNTs are, the greater are the contact area between parallel CNTs and the greater are the intermolecular forces between two CNTs. It is estimated that to achieve fibre strengths near the intrinsic strength of CNTs, the CNT contact length must be in the order of 10 to 120 μm. Today though, the typical length of CNTs are only 300 nm, meaning that the strength of fibres are only a fraction of what is possible [Goddard, 2003].

Nano memory

CNT random-access memory, or for short NRAM, is a new type of electronic memory developed by Nantero, that can be used in computers, cell phones, MP3 players, digital cameras and PDAs. In this type of memory the extraordinary tensile strength and resilience of CNTs are utilized to store data.

The structure of a memory cell is illustrated in Figure 2.13 where it can be seen that the CNTs are serving as addressable electromechanical switches arrayed across the surface of a microchip. The CNTs act as relays, which can stay in a straight position representing a 0 and in a bended position representing a 1. To store a 1, an electric field is applied. This forces the CNTs to flex downward into a depression etched on the surface of the microchip. Once the CNTs are bended they can stay in this position even when the electric field is turned off. The CNTs does not flex back due to the van der Waals interaction forces between the CNTs and the surface of the microchip. The utilization of this interaction makes NRAM energy efficient.

To erase the stored bit an electric field of different polarity is applied. This causes the CNT to return to its straightened position [Stix, 2005]. The bits can be read by applying a weak electrical current which has to be weaker than the one used to write the bits. The reason for this is that a strong reading current will spoil the data already written to the chip. The reading process is described in Figure 2.13 and as illustrated, the modules of CNTs are connected in linear tracks that bridges the gaps over the electrodes. These electrodes are placed orthogonal under the linear tracks. To read a track a weak positive pole are connected to the CNT tracks. The system can now be read by connecting a negative pole to one of the electrodes. If there is contact between the two layers the current flows meaning that 1 has been stored. If contact is not established, no current flows and it will read as 0. Now the next electrode can be charged and such on all the way to the end of the track. Then the next track can be charged and the process starts all over.

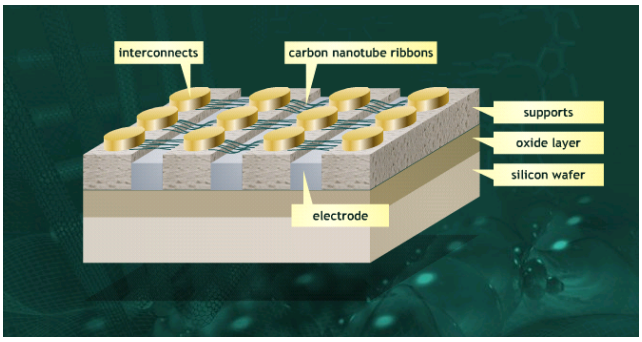

Figure 2.13: The surface and construction of a NRAM chip [Stix, 2005]

According to Nantero this technique might make it possible to store hundreds of gigabits or maybe terabit on a microchip [Nantero, 2005]. To realize the idea of using CNTs in NRAM, Nantero had to overcome two problems. First of all, the amount of iron particles had to be reduces as they could produce undesirable tremors in the

further production. Nantero developed a complex filtration process, which reduces the amount of iron to the parts-per-billion level. The second problem was how to place the CNT in the right places on the microchip. Deposition of CNTs onto the wafer using gas vapor was not possible because this process requires temperatures at about 1000 degree. This high temperature would ruin the already placed circuitry. The Nantero ended up using a coating technique where a CNT-containing solvent is spin coated onto the wafer. This technique leaves a thin film of CNTs on the wafer after the solvent is removed. Afterwards are lithography and etching used to form the right pattern of CNTs. According to Scientific American the first commercial production of NRAM will take place next year [Stix, 2005].

CNTs in Light Bulbs

In June 2004, Chinese scientists managed to produce a light bulb based on highly purified CNT filaments, instead of the traditional tungsten filaments used today. The original tungsten filament was replaced by a CNT filament in an ordinary 40-watt light bulb. The scientists found that the CNT filament emitted even more light than traditional 40-watt light bulbs. Furthermore, the CNT filament had a lower threshold for light emission than tungsten filaments. Another quite exciting discovery made by the scientists was that the CNT filament did not change its resistance at temperatures up to $1750K$. This discovery suggests that CNTs could someday be used as high precision resistors. [Dumé, 2005]

2.9 Orbital shapes

Orbitals are models, which describe the probability distribution of the electron around the nucleus in an atom. According to Pauli's exclusion principle each orbital can only contain two electrons of opposite spin. The number of orbitals attached to each electron level in an atom is equal to the second power of the level number. The orbitals in each level are divided into subshells, which are marked s, p, d, f and g. In the first level there is only room for two electrons, which means only s orbitals occur in the first level. The p orbitals are added in level two, d orbitals in level three, f orbitals in level four and finely g orbitals in level five. The number of orbitals attached to each subshell is starting with one orbital in subshell s and rises by two from subshell to subshell. The shape of the s- and p-orbitals are illustrated in Figure 2.14.

As seen in Figure 2.14 the s and p orbitals are marked with $2s$, $2p_x$, $2p_y$ and $2p_z$. 2 refers to which level the orbital belong and the letters x, y and z tells the orientation in proportion to the system of coordinates. The two first types of orbitals are relatively simple to draw but the shape become more complex for the other types of orbitals.

CNTs are build from carbon atoms and it is therefore important to know the electron structure of these to get a better understanding of the CNTs and their bindings. Carbon has the atomic number 6 and therefore has 6 electrons, which

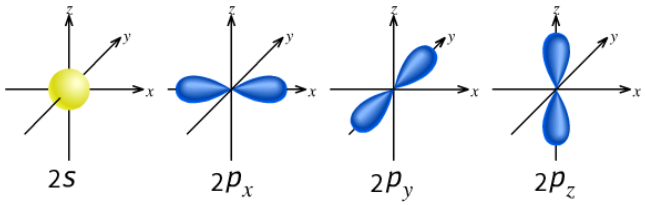

Figure 2.14: The orbitals belonging to the second principal quantum number [mhhe.com, 2005].

means the electrons are placed in s and p orbitals. The first two electrons fill up the $1s$ orbital. The last four electrons, which also are the valence electrons, are placed in the following way. Two electrons in the $2s$ orbital and two electron in $2p$ orbitals. The carbon atoms in CNTs are bonded together by covalent bonds, which normally are described as a system where the atoms are sharing the valence electrons. The covalent bonds can also be described more detailed with atomic orbitals used to share the valence electrons. The crystal lattice of CNTs can be seen as a rolled up graphene sheet and therefore it will be assumed that the bonds between the carbon atoms are similar to the bonds in graphite. In graphite all the carbon atoms are organized in plane lattices consisting of hexagons where all the $C-C$ bonds are known to be equivalent. To explain this fact, the three double bonds must continuously shift between the carbon atoms in the hexagon. As mentioned before the valence electrons are placed in $2s$ and $2p$ orbitals, which mean there can be four overlaps of orbitals. These overlaps can be between to identical orbitals or between a $2s$ and a $2p$ orbital.

However these overlaps will give a formation that does not corresponds to the real formation where each carbon atoms are bonded in the plane to three other carbon atoms with an angle of 120 degrees. To overcome this problem it makes sense to assume that the carbon atoms use orbitals, that are combinations of $2s$ and $2p$ orbitals. In fact a combination of a $2s$ orbital and two $2p$ orbitals makes three orbitals in the plane with an angle of 120 degree between each other as it can be seen in Figure 2.15.

This mixing of the original orbitals to form special orbitals for bonding is called hybridization. The three new orbitals are called sp^2 because they are hybridization of one $2s$ and two $2p$ orbitals (s^1p^2). After this hybridization of orbitals it is possible to explain the bonds in the carbon hexagons where there exist two types of bonds. The first type of bonds is the sigma σ bond, which is a bond between two sp^2 orbitals. In this bond the orbitals are overlapping each other and it occurs between all the carbon atoms. The second bond is a π bond, which in this is called a delocalized π bond because of the electron resonance. The π bond is formed between two $2p$ orbitals as it require less energy compared to a bond between two $2s$ orbitals. In this π bond the shared electron pair occupies in the space above and below the plane of the σ bonds [Zumdahl and Zumdahl, 2003]. In the case of the CNTs the curvature and the folding angle of the graphene layer determines if the specific (n, m) folding

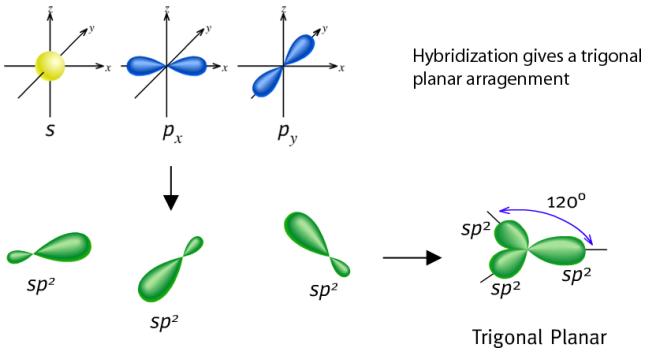

Figure 2.15: The hybridization between $2s$, $2p_x$ and $2p_y$ orbitals. The figure is modified from [mhhe.com, 2005]

of the tube gives conducting or semiconducting properties. The reason for this is that the p orbitals interacts with each other.

2.10 Crystalline structure

A crystal is matter in the solid state where the atoms are ordered in a periodic arrangement. Ideally, it is an infinite repetition of identical atoms or of a structure of atoms. In Figure 2.16 the definition of a crystal is described. The crystal can be described as if the bases where attached to points in a lattice. [Kittel, 2005]

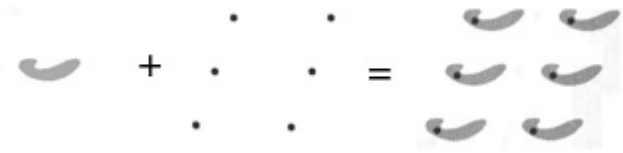

Figure 2.16: The basis is added to the lattice forming the crystal. Note that the lattice is a net in three dimensions, while only two dimensions are displayed here. $Basis + Lattice = Crystal$. Modified from [Kittel, 2005]

It does not matter if the lattice is displaced as long as it fulfils the criteria of the lattice definition. The points of the lattice are defined by the addition of the translation vector to one point of the lattice:

$$R1 = R + \mathbf{T}, \mathbf{T} = n1\mathbf{a1} + n2\mathbf{a2} + n3\mathbf{a3} \tag{2.7}$$

a1, **a2** and **a3** being the unit vectors of the lattice and $n1$, $n2$ and $n3$ being arbitrary integers. The translation vector, **T**, describes the difference between the two points, R and $R1$. The relation between two points, when suitable numbers, $n1$, $n2$ and $n3$ are chosen, can be described by the translation vector. This means that the lattice units are the smallest possible. Several lattices may be chosen for

one crystal. For either choice the same results of analysis including x-ray diffraction pattern ensue as long as the translation vector of Equation 2.7 has been satisfied. The crystal can be defined with basis in the growth of bases on top of each other or from a given lattice as long as Equation 2.7 is maintained.

In a lattice it is possible to chose several different unit cells, however, a distinction between the primitive unit cell and the unit cell is necessary. The primitive unit cell is defined as minimum volume cells. Each primitive cell has only one lattice point attached and for a given crystal the number of atoms in the primitive cell is invariable. A normal choice of primitive cell is the parallelepiped. In Figure 2.17 different primitives cells, cell 1, 2 and 3 and one nonprimitive cell 4, are shown. [Kittel, 2005]

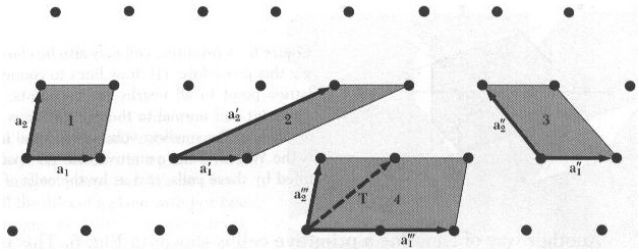

Figure 2.17: The choice of different unit cells is possible. 1,2 and 3 are primitive cells while 4 is not.[Kittel, 2005]

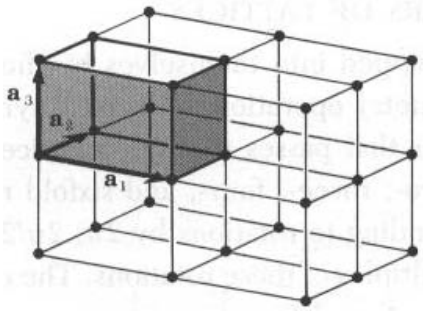

Figure 2.18: The cell determined by the vectors a1,a2,a3 is a primitive parallelepiped unit cell [Kittel, 2005].

For a parallelepiped primitive cell, see Figure 2.18, the number of lattice points touched by the primitive cell is 8, and when neighboring 8 identical cells the number of associated lattice points must be: $8 \cdot 1/8 = 1$.

Wigner-Seitz Cell

One way of choosing the primitive cell is the Wigner-Seitz cell. Lines are drawn to connect a chosen lattice point to all nearby points. At the midpoint new lines or planes are drawn normal to the first lines. The smallest volume enclosed by the

lines or planes drawn is defined as the Wigner-Seitz cell and it is a primitive unit cell. See Figure 2.19 for an illustration of this method. [Kittel, 2005]

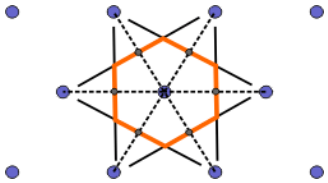

Figure 2.19: The primitive unit cell constructed by the Wigner-Seitz cell.

Reciprocal space

The reciprocal space is encountered when using quantum mechanics or Fourier analysis. It is called either reciprocal space, the wave space or k-space from either the unit of the axes or the origin. Due to the periodicity of crystals functions of an equal periodicity is required to describe the electronic structure. This yields that the points in the reciprocal space are determined by $2\pi p/a$, $p \in Z$. See Section 2.13 for more about the wavefunction of electrons. The unit cells of the reciprocal space are given by:

$$\mathbf{b_1} = 2\pi \frac{\mathbf{a_2} \times \mathbf{a_3}}{\mathbf{a_1} \cdot \mathbf{a_2} \times \mathbf{a_3}}; \mathbf{b_2} = 2\pi \frac{\mathbf{a_3} \times \mathbf{a_1}}{\mathbf{a_3} \cdot \mathbf{a_2} \times \mathbf{a_1}}; \mathbf{b_3} = 2\pi \frac{\mathbf{a_1} \times \mathbf{a_2}}{\mathbf{a_1} \cdot \mathbf{a_2} \times \mathbf{a_3}} \tag{2.8}$$

A Wigner-Seitz cell in the reciprocal lattice is defined as a Brillouin zone. Hence, the first Brillouin zone is the primitive cell in the reciprocal lattice. [Kittel, 2005]

2.11 Conducting Properties of Solids

In solid state physics the electrical conductivity of crystals is divided into three classes: conductors, semiconductors and insulators. In this section the difference between these three classes will be discussed in terms of models based on energy bands.

Fermi Levels

The value of the Fermi level at $0K$ is called the Fermi energy and is a constant for each solid. According to the Pauli exclusion principle each energy level can accommodate only two electrons. Hence, at $0K$ the electrons pack into the lowest possible available energy states and build up a Fermi sea of electron energy states. The surface of the sea is the Fermi level where no electrons at absolute zero will have enough energy to rise above the surface. The Fermi level is any energy level having the property that it is exactly half filled with electrons. Levels of lower energy than the Fermi level tend to be entirely filled with electrons, whereas energy levels

higher than the Fermi level tend to be empty. The Fermi energy E_F for an electron restricted to motion in one dimension is defined in Equation 2.9

$$E_F = \frac{\hbar^2}{2m}\left(\frac{N\pi}{2L}\right)^2 \tag{2.9}$$

Where N is the total number of electrons and L is the length of the line to which the electron is confined. For more information about this model see Section 2.12.

As the temperature rises or as electrons are added to or withdrawn from the solid the Fermi level changes and a certain fraction of electrons will exist above the Fermi level. This is characterized by the Fermi-Dirac distribution function. [Kittel, 2005]

Fermi-Dirac distribution function

The Fermi-Dirac distribution function $f(E)$ gives the probability that a given available electron energy state E is occupied by one of the electrons in a solid. It is given by Equation 2.10.

$$f(E) = \frac{1}{e^{(E-E_F)/k_bT} + 1} \tag{2.10}$$

where k_b is Boltzmann's constant and T is the temperature measured in Kelvin.

The left figure in Figure 2.20 is a plot of $f(E)$ versus E for $T = 0K$ and it shows that $f(E) = 1$ for $E < E_F$ and that $f(E) = 0$ for $E > E_F$. This illustrates, as explained in Section 2.11 that at $0K$ all states with energy less than the Fermi energy are occupied and all states with more energy are unoccupied.

The figure to the right of Figure 2.20 is a plot of $f(E)$ versus E for $T > 0$ and it shows that as T increases, the distribution slightly rounds off. Due to thermal excitation states near and below E_F lose electrons and states near and above E_F gain electrons. [Kittel, 2005]

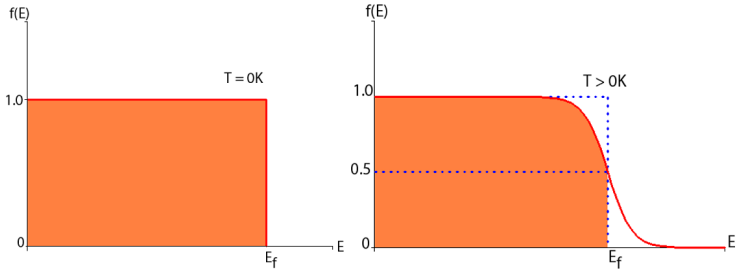

Figure 2.20: Plot of the Fermi-Dirac distribution function for $f(E)$ versus E. To the left is a figure of $T = 0K$ and to the right $T > 0$.

Metals

Metals are good conductors because the charge carriers, the electrons, are free to move in response to an applied electric field. When an electric field is applied to a

metal, the energy of the system will be increased, which corresponds to the additional energy of the moving electrons. Therefore, when an electric field is applied to a metal, electrons must move upward to a higher available energy state in an energy-level diagram. The bottom most energy band in Figure 2.21(a) illustrates a alf- filled energy band in a conductor at 0 K, where the blue region represents levels filled with electrons. The electrons in the band obey the Fermi-Dirac statistic, which means all energy levels below the Fermi energy (E_F) are filled and no one above is filled. The Fermi energy lies in the band at the highest filled state. This distribution only occurs a 0 K, and electrons can thermally be excited to levels above E_F if the temperature is increased slightly. This means the electrons, having energy near the Fermi energy, only needs a small amount of additional energy to reach an empty energy state above the Fermi energy. Therefore, electrons in a metal can be free to move when a small electric field is applied [Serway and Jewett, 2004].

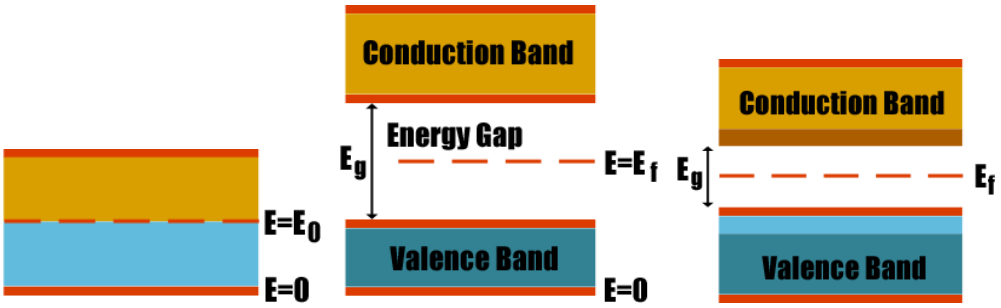

Figure 2.21: The band structure of (a) a metal (b) an insulator and (c) a semiconductor.

Insulators

The difference between a metal and an insulator is that the energy band in an insulator is not continuous like in a metal. The energy band of an insulator is shown in Figure 2.21(b). The highest filled energy band is called the valence band, and the lowest empty energy band is called the conduction band. The energy separating the valence band and the conduction band is normally referred to as the energy gap or band gap. The energy gap occurs because there are no allowed energy levels in this area. The Fermi energy lies somewhere in the energy gap as shown in the figure. It was earlier mentioned that the Fermi energy lies in the band at the highest filled state, and this might suggest the same placement in an insulator. The reason why the Fermi energy is placed between the bands in an insulator can be explained by a more sophisticated treatment of the Fermi energy. The presence of the energy gap is also the reason why an insulator cannot lead a current. The energy required to excite an electron from the valence band to the conducting band is too big to be obtained by applying an electric field. Therefore free moving electrons cannot be obtained in an insulator.[Serway and Jewett, 2004]

Semiconductors

The band structure of a semiconductor is illustrated in Figure 2.21(c). Like an insulator a semiconductor have an energy gap between the valence band and the conducting band. The difference between an insulator and a semiconductor is the size of the energy gab. The Fermi energy is placed between the two bands like in an insulator. At 0K all the electrons in a semiconductor are placed in the valence band. When the temperature increases, an appreciable numbers of electrons are excited into the conduction band because the energy gap is not as large as in an insulator. There are many empty levels above the thermally filled levels, which means that a small electric field can raise the electrons in the conducting band, resulting in a moderate current. [Serway and Jewett, 2004]

2.12 Energy of the nearly free electron

The origin of band gabs can be explained using the model of the nearly free electron. In order to describe this model the first thing is to look at the model of the free electron. Consider an electron existing in a space without any influence from other particles. Looking at this electron from a quantum mechanical point of view the time-independent Schrödinger equation in one dimension is of much interest. This equation is used to determine the wavefunction which describes the energy for quantum mechanical systems. See Equation 2.11.

$$-\frac{\hbar^2}{2m}\frac{d^2\psi}{dx^2} + U\psi = E\psi \tag{2.11}$$

In this equation $\hbar$ is Planck's constant divided by 2π, m is the mass, E is the energy of the electron and ψ is the wavefunction. In the case of the free electron the potential U is equal to zero. The solution of this equation is, in the case of the free electron, on the form seen in Equation 2.12.

$$\psi_k(x) = e^{ikx} \tag{2.12}$$

Equation 2.12 describes a wave, hence the description as a wavefunction. In relation to quantum mechanics the solutions of these wavefunctions will often be divided in two groups of functions; allowed and forbidden functions. The forbidden functions are those at which the wavefuntion is different from 0 at the barriers. The division into allowed and forbidden functions will be further described later on in this section. In the case of the free electron there are no forbidden values of the wavefunction. The plot of the energy as a function of the wavevector k will form a parabola stretching from zero to infinity. [Kittel, 2005]

Looking at the model of the nearly free electron, compared with that of the free electron, there are one major difference. The nearly free electron is restrained by boundaries from the nucleus it orbits. As a result of this, only some of the wavefunctions will be allowed. In order for a wavefunction to be allowed it is necessary that

the space defined by the model allows for either half or whole wavelengths to exist in the space. In Figure 2.22 a model of the probability distribution of the nearly free electron potential well is illustrated and it includes the square of the three first legal wavefunctions.

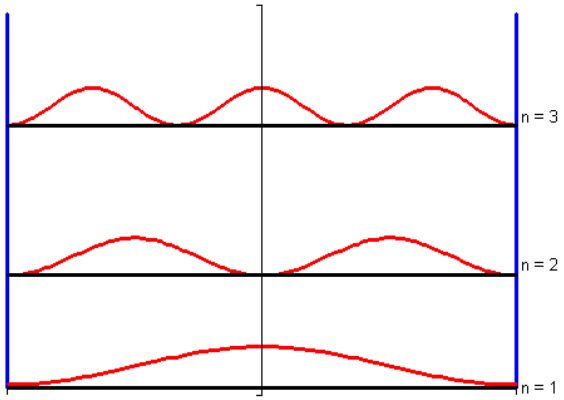

Figure 2.22: A model of the probability distribution of the nearly free electron where the legal wavefunctions are plotted. The x-axis describes the position of the electron in relation to the nucleus and the y-axis plots the probability of finding the electron in the given position. The horizontal lines plotted in connection with the wavefunctions is the energy belonging to the specific wavefunction. The boundaries at the end of each wavefunction is infinitely.

From the model it is seen that the individual wavefunction belongs to a specific energy. The energy levels between the plotted functions, not occupied by a wavefunction, is the earlier mentioned forbidden values. These unoccupied energies explain the phenomena of band gabs. If the electron of the system exists at the first legal energy level $n = 1$, the minimum energy needed to excite the electron to the next legal energy level $n = 2$ is the difference in energy between the two levels ΔE, hence the size of the band gab.[Kittel, 2005]

2.13 Electron in a crystal

In order to achieve a realistic image of the band gab in a CNT it can be advantageous to investigate the model of an electron in a crystal. A CNT is constructed of a series of primitive cells defined by the two vectors $\mathbf{C_h}$ and $\mathbf{T}$. This is basically a one dimensional crystal with a complicated basis. The method of calculating the conducting properties is comparable with the method used in a simple 1-dimensional crystal.

The potential energy in this one dimensional model varies with the distance to the nucleus in accordance with the coulomb force. An approximated model with quadrangular potential wells can be used in order to simplify the calculations re-

sembling multiple potential wells of finite size on a line. This model is shown in Figure 2.23 along with the borders of the Wigner-Seitz cell.

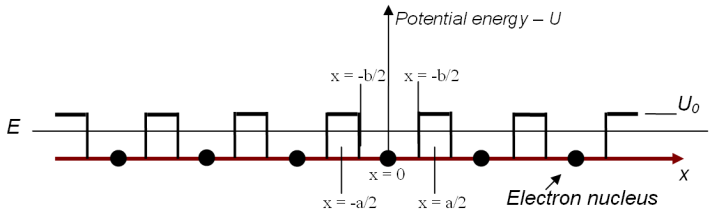

Figure 2.23: The potential energy U is shown on the y axis of the crystal. The black spheres are the atom nuclei, the E level displays the energy of the electron which is set below the potential energy between the atom nuclei. The first Weigner-Seitz cell is between $x = -\frac{a}{2}$ *and* $x = \frac{a}{2}$.

According to the assumption of infinite length, translational symmetry exists and the potential energy and the probability density must be periodic with the period a. Because the probability density of electrons is measurable this is the solution which is found. A periodic probability density can be achieved by multiplying a periodic function by a complex number of modulus 1:

$$|\Psi(x)|^2 = |\Psi(x+a)|^2 \tag{2.13}$$

$$\Psi(x) = e^{ikx} \cdot \psi(x) \tag{2.14}$$

Furthermore, there is no change in the probability density from x to $-x$ so the wavefunction $\Psi(-x)$ must be equal to either $-\Psi(x)$ or $\Psi(x)$. The final solution must be a linear combination of these functions. They are named $f(x)$ and $g(x)$ respectively. From considerations in continuity at $x = \frac{a}{2}$ compared to $x = -\frac{a}{2}$ the following equations can be derived:

$$\cos(ka) = \frac{fg' + f'g}{fg' - f'g}|_{x=\frac{a}{2}} \tag{2.15}$$

The solution to this is real when $|\cos(ka)| \leq 1$. Values out of this range is called the band gap. For the chosen well model it is possible to derive expressions for f and g through the Schrödinger equation and after insertion in Equation 2.15 the following expression for $\cos(ka)$ can be derived:

$$\alpha = \frac{\sqrt{2mE}}{\hbar}\,,\ \beta = \frac{\sqrt{2m(U-E)}}{\hbar}\,,\ \beta' = \frac{\sqrt{2m(E-U)}}{\hbar} \tag{2.16}$$

$$\cos(ka) = \cos(\alpha b)\cosh(\beta(a-b)) + \frac{\beta^2 - \alpha^2}{2\alpha\beta}\sin(\alpha b)\sinh(\beta(a-b)), E < U \tag{2.17}$$

$$\cos(ka) = \cos(\alpha b)\cosh(\beta'(a-b)) + \frac{\beta'^2 - \alpha^2}{2\alpha\beta'}\sin(\alpha b)\sinh(\beta'(a-b)), E > U \tag{2.18}$$

These two expressions are plotted in Figure 2.24 showing the allowed and forbidden energies of the electron. The grey regions represents forbidden energies (band gaps) and the white regions represent allowed energies. Each energy corresponds to a value of k, and thereby some values of k becomes allowed and some forbidden.

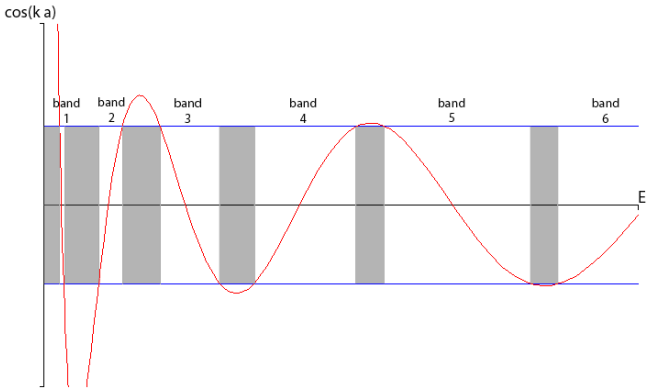

Figure 2.24: Equation 2.18 is plotted as a function of the energy of the electron. Only energies that correspond to a $\cos(ka)$ *value between* -1 *and* 1 *are allowed. Note that each band and bandgab corresponds to a band of allowed and forbidden k values, respectively.*

With Equation 2.18 it is possible to derive an approximated expression for the energy band of electron. This is only precise for narrow bands and is displayed in Figure 2.25. Next to this figure two energy bands for CNTs are displayed as a comparison.

In each energy band there can be two electrons of opposite spin according the Pauli's exclusion principle. The six electrons of carbon must therefore be divided in 3 full bands. This makes the tetrahedral structure of diamond an insulator. The Π orbital of graphite is responsible for the conducting properties which are also present in CNTs.

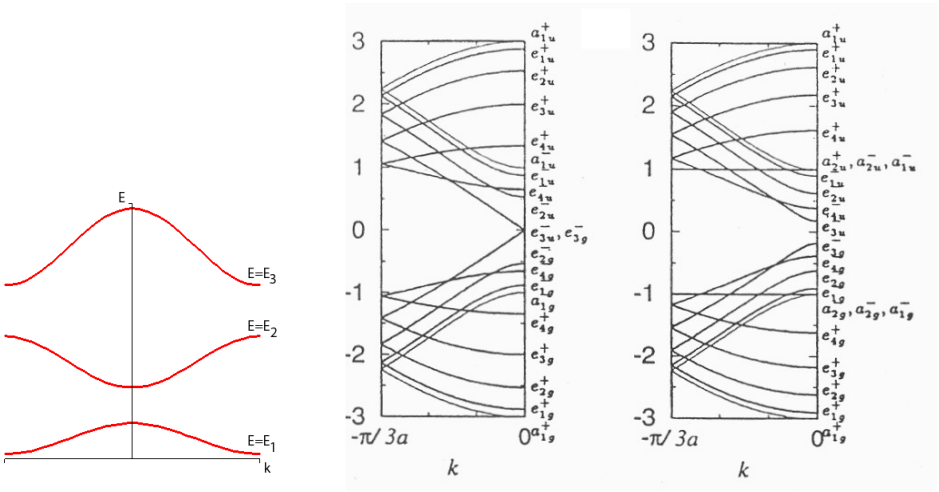

Figure 2.25: The left image displays the energyband of the simple 1D crystal. In the middle and to the left the band gap of a (9,0) zig-zag metallic and (10,10) zig-zag semiconductor CNT are displayed respectively.

2.14 Project Limitations

The approach to this project is CNTs in relation to nanotechnology. The initiating problem "Which problems concerning integration of CNTs in products exists?" sets some limitations towards the contents of this report. This means that production of CNTs will not be a part of this project. Instead the focus will be placed on the following sub areas: separation-, analysis and characterization of CNTs. In order to obtain data about the properties of CNTs, it is necessary to separate the CNTs from each other. This is done to prevent analyzing the bundles that CNTs naturally form due to van der Waals interactions. In this context a method from 2002 will be tried out. In relation to the different analyses that will be performed on the CNTs, the following properties are relevant to examine: electrical-, vibrational-, mechanical- and optical properties. In this project it is not possible to investigate the mechanical properties, such as strength and deformation caused by external forces, of the CNTs, due to lack of appropriate equipment. With respect to the electrical properties it is not possible do determine if the single CNT is conductive or semi conductive. By using SEM and AFM, it is possible to achieve typographic data of a surface prepared with CNTs, and can be used to determine if the CNTs are separated from the bundles. Furthermore the size of the CNTs can be estimated by means of these two methods. The optical properties can be examined by using absorbance- and fluorescence spectroscopy. The vibrational properties can be examined using FTIR- and Raman spectroscopy. To sum up, the methods which will be used are: atomic force microscope, scanning electron microscope, fluorescence spectroscopy, absorption spectroscopy, fourier transform infrared spectroscopy and Raman spectroscopy. The data from these methods can be used to describe the atomic configuration and properties of the CNTs.

2.15 Problem Statement

The purpose of this project is to analyze the structure and properties of CNTs. In order to do this a quantum mechanical perspective must be applied. Furthermore the purpose of this project is to evaluate on the conducted experiments and their validity.

- Why is it necessary to use quantum mechanics instead of classical mechanics?
- How is it possible to separate the bundles which CNTs form in a solution?
- How can the electrical properties of CNT be determined?
- How can the diameter distribution be determined?

Chapter 3

Methods and Validation

3.1 Change of Paradigm

The ancient Greeks are said to be the ancestors of modern science. There are two main reasons of this postulate. They were the first to separate logical thinking from the organized religion and they formed the basis of empiric science. [Brier, 1994]

The Greek view of the world was based on the concept of the four elements; earth, fire, air and water. Though this appears to be very primitive, the basic thought of the world being build from small building blocks is the same as the theory of today. These basic concepts of finding a hidden logic behind occurrences and matter has made seeds for further advancement in the field of science.

Two Greek mathematicians, Aristotle and Euclid, must be mentioned because their work made basis for the development of the empiric scientific method and the basis of geometry.

Aristotle is basing his theses on characteristics found by observation rather than philosophical thinking and thereby separating himself from his contemporaries. He distinguishes between events that *"sometimes but not necessarily occurs"* and those that *"always or often occurs"*. By using these significant occurrences he divides events into classes. This introduction of empiric science is the basis of the modern experimental science. Aristotle thereby made a milestone in the history of science. [Brier, 1994]

From 10 basic postulates Euclid wrote the work Elements. The first books covering the subjects from basic plane geometry, including the ratio later known as the golden section, through elements from number theory ending with three dimensional figures and the platonic solids in book XIII. The principle with basic postulates, later known as axioms, inspired the axiomatic method of modern mathematics, which was further developed by Newton. [www.britannica.com, 2005].

The primary objective of the Greek science was to understand how the world functions based either on philosofical thinking or observations. This has also been the goal of the later science.

In the beginning of the 17th century Galilei shaped the principles of the modern

mechanical science.

- Firstly, he specified the principle of observation, introduced by Aristotle, from being observations, into a way of measuring properties. This states his realization of the subjective character of our senses.
- Secondly he introduced a mathematical aspect in physics implying that physical laws could be expressed by mathematical symbols and equations.
- Thirdly he developed the idea that the world consists of small indivisable parts, the smallest indivisible part of matter, and made this thought integrated in the public society.

Newton further developed the mechanical science and published his three famous laws of motion. These laws fully determine the motion and position of an object at any given time, from the knowledge of its initial location, speed and forces acting on it. This leads to the belief that if these factors are known for all particles in a system, the motion of the object in the future and in the past are determined and can be calculated.

The famous scientist Albert Einstein is behind one of the most significant new theories in the 20th century. He drastically ruined the thought that time and space are independent, by introducing a correlation between time and space now known as the relativistic laws of motion. This dramatically changed the understanding of fundamental quantities like mass and time, as they are now functions of the speed of the object. This theory was however introduced in order to make the physical laws valid in every situation and inertial system. The newtonian laws can be seen as an approximation that is accurate at velocities up to 10% the speed of light. Einstein's ambition was to increase the understanding, logic and predictability of the world. [Brier, 1994]

Quantum mechanics destroyed the vision of ultimate predictability, logic and perhaps also understanding of the subatomic elements disabling the validity of the newtonian laws of motion. A smallest step was introduced for both motion, energy, location etc., along with making it impossible to determine the exact location and velocity of an object. Precise and almost holy laws of motion was replaced by probabilistic calculations, where quantities like velocity and position cannot simultaneously be known exactly. Quantum mechanics predicts the quantization of energy, and introduces energy as being allowed only in discrete packets of a certain size.[Brier, 1994]

The Schrödinger equation introduced the wavefunction of the electron. When squared, it tells the probability density of the electron. The Schrödinger equation is a differential equation and solving it exactly is often not possible, and numerical solutions are required. Among other things, the wavefunction allows us to calculate the electronic density of a material. This can be used to determine the bandstructure which is accountable for many of the thermal and electrical properties.

This way of thinking introduced by quantum mechanics is transparent to our everyday life, because everything can be seen as continuous at macroscopic scales revalidating the relativistic laws of motion. At atomic scale however the path of the electron orbiting the nucleus cannot be determined neither theoretical nor experimental. At any given time t, the location of the electron and the momentum can be determined but this reveals nothing about the location or momentum at $t + \Delta t$. Heisenberg even put a theoretical limit to how precise the momentum and location of the particle can be determined. If determining the location exact the momentum will be infinitely imprecise and vice versa.[Brier, 1994]

In opposition these theories are crucial for the description of nanoscale structures. The movement is limited within a few nanometers resulting in discrete allowed energies. A quantum mechanical description is needed to explain phenomena like the electrical and optical properties of CNTs.

This description has also entailed the development of measuring instruments using quantum mechanical effects. In scanning electron microscopy the wave-particle duality of electrons are used to scan a surface and the Raman effect in inelastically scattering of light is used in Raman spectroscopy.

Quantum mechanics are not logical compared to the classic physics. It was and still is a problem for some scientists to accept that the basic occurrences in the universe cannot be described exactly by any physical law. Einstein and Bohr have had this discussion. “I refuse to believe that God is throwing dices, and that the fundamental properties of matter cannot be expressed by nothing but a probabilistic description.”, Einstein said. Bohr replied, “Do not tell God what to do”. Einstein was so firm in his belief, that the fundamental connections could be found through a mathematical and logical description, that he could not accept the quantum mechanical description. Bohr is on the other hand accepting this explanation, as it removes all contradictions leaving the fundamental unexplained. [Brier, 1994]

The hunt for the Theory of Everything is however not over. Superstring theory is in the lead for a unifying theory as it reduces the amount of basic particles and forces drastically. In this theory multiple dimensions are added and the building bricks of the universe are small strings, only $10^{-35}m$ long. Different vibrational modes would yield different particles. Although this theory reveals some basic relations entails the addition of 6 to several hundred dimensions.[Brier, 1994]

Although quantum mechanics was a setback in the vision of finding the fundamental relations in nature, it has been successful in explaining several phenomena on the atomic scale. The search for the basic understanding of everything has continued in the superstring theory.[Brier, 1994]

3.2 Scientific methodology

The objective of scientific methodology is to conclude how reliable the scientific knowledge is. These considerations are necessary when dealing with scientific methods, and it is necessary to be aware of the reliability and validity of the methods

being used.

Science

Science as a concept is a very diffuse or maybe, a rather wide scaled size. Science can be spoken of in many different ways and within many different areas of specialization, such as science of nature or social science. These groups can furthermore be divided into several directions. A short description of science can be "The activity at scientific institutions", where the term institution can be defined as "A system of rules, expectations and assumptions which controls and are the basic of the individuals' choice of activities in regard to other people, objects and actions". From this follows that science is a general statement and way of expressing all results, positive or negative. This is the outcome of the work that students, scientists and others daily deal with on scientific institutions such as universities or other institutions of higher education. However, knowledge can also occur at, for instance, places with financial interests without being a product of scientific research. [SME, 2004]

Science can be split into different levels depending on the goals and basis of a study or article, as the target group is different in each case. It is important to distinguish between communication, development and research when one speaks of science.

Procurement of knowledge, as for example science journalists are engaged with, is helping new knowledge to reach the society, and here the author knows both the question and the answer in advance. In development experiments the question is known, but the answer is not. This is what one is looking for. In contrast to this is research, where neither nor the question is known in advance.

The purpose with the expansion of science in the society in general is probably due to human nature, which encourages development in many aspects. By developing new knowledge in the form of reports, thesis', articles and also candidates, science enhances the productivity and efficiency and thereby the competitive position of the companies in the society. Also, the individual human being have a desire to expand knowledge, as new knowledge always opens new questions science is extended naturally. [SME, 2004]

In general science summarizes the demands of human beings to produce new and extend existing knowledge by choice or accident.

3.3 Methods

When working with science it is important to know and to be familiar with the scientific methods which justifies examinations and measurements to be ascribed as valuable and scientific work. Logic and methodology are therefore important basic subjects in the traditional fields of science such as mathematics, physics and chemistry. These fields build upon principles from logic and methodology. In this section the methods used in the examination of CNTs will be further described. [leksikon.org, 2004]

The general method which has been used throughout this project is known as the hypothetic-deductive method, which is a well known and regularly used method in scientific work. The method can be described graphically as illustrated in Figure 3.1. The starting point is a hypothesis that is tested empirically. If it cannot reject the hypethesis during the empiric test, a theory can be formulated. If, however, the hypothesis is rejected it must be revised before another empirical test. [leksikon.org, 2004]

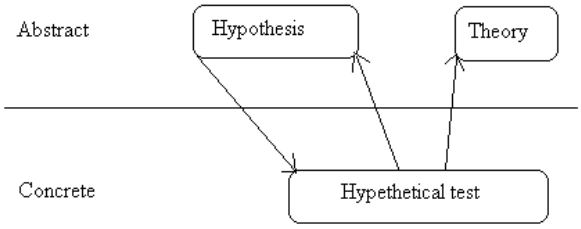

Figure 3.1: The hypothetic-deductive method. A hypothesis is formulated and tested, and eventually either rejected or confirmed.

The hypothetic-deductive method will be further described in the following sections.

A general view on the scientific principles in connection with methodology will be the first subject. Basically, methodology is a subject which is used to determine the scientific value of a certain piece of scientific work or examination. Furthermore, the methodology is used to establish delimitations. [Føllesdal et al., 1995]

Phases of methods and observations

Normally the natural scientific methodology is separated in phases. The individual phase can be ascribed different levels of attention determined by the extend and purpose of the work. The phases can be arranged as follows:

Observation - Development of hypothesis - Test - Way of communication

This arrangement is not optimal for this project. Due to a rather narrow time frame, and because knowledge and theories about CNTs already exist, the work and examinations of this report will be based on testing the hypothesis developed- and observations done by others. Therefore the focus will be placed on testing the hypothesis'. Furthermore the principles of communicating the results will also be focused on in this report.

While working with nanotechnology it is especially interesting to deal with the subjects of observation and methodology. On the nanoscale the human senses are not of much use. This means that different instruments must be used to make indirect measurements. Because it is not possible to make direct observations on

the nanoscale, it is difficult to tell if the results can be trusted. Sources of error in connection with measurements on the nanoscale can be many, varying from flaws in instrument construction to more obvious problems such as the coloration contrast of for example SEM and AFM pictures. Another aspect leading to errors is that the human senses and brain is in use while interpreting the data. [Føllesdal et al., 1995]

In general it can be said that observations of objects in the perspective of nanotechnology are a combination of different factors such as the sense impression a person gets, the sensing organ used, mainly the eyes, because it is the eyes that reads the results. This again depends on the used instrument and finally the analyzed object itself. Because of this it is necessary to apply methods that can eliminate errors and uncertainties. This can for example be intersubjective control, where a number of persons observe the same subject under the same conditions. The different observations are then compared to get an averaged observation. Another way is to use reiteration control where the single examination is carried out a number of times, letting the average value be an expression of the "true value" and basing the conclusion on the averaged result. [Føllesdal et al., 1995]

The set up and test of hypothesis

A hypothesis is a scientific assumption, from where consequences can be deduced. This makes a contrast to another type of hypothesis called inductions which is the same as generalizing. A deduction is used to predict new observations, and these hypothesis' are called existence hypothesis'. The methods used in the examination of CNTs can be described through the hypothetic-deductive method. As the name indicates the theory is deduced from a certain hypothesis. From this deduction the theory is tested and as a result of this testing the theory can be either verified or rejected. In this report the starting point for the experiments will be a theory or a prediction which tells how the outcome of the experiment will be. Test of an hypothesis is an important part of scientific work and this is done in the examinations of CNTs in this project. Because direct observations cannot be made, it cannot be verified if it is really CNTs which are being observed, it can only be assumed. From this assumption several experiments can be setup to verify the presence of CNTs. An existence hypothesis, as those dealt with in this project, can be verified if the predictions are found to be true. In nanotechnology a problem with this verification occurs. As a result of the nature of nanotechnology it is often not possible to verify the hypothesis directly, and verification can only be done indirectly. This is for example the case with the data of the IR-spectroscopy experiment where the output of the experiment cannot document the presence of aromatic systems, but with an element of uncertainty can conclude that they are present. This method of verification is of course not certain and as a result of this, the conclusions on the hypothesis' based on the experiments will be careful. If the results obtained are in conflict with the hypothesis', it is more likely to be due to impurities in the sample and errors made under the conduction of the experiment, than because of a wrong hypothesis. Therefore completely verification or rejection of the hypothesis' cannot

be done in this project [Føllesdal et al., 1995]

Way of communication

Scientific way of communication stand in contrast to the everyday communication. This is due to the contents in scientific work such as reports and articles. This needs to be formulated precise so that other scientists can analyze the contents and replicate the exact situation and get the same result as the author of the article. The scientific way of communicating is therefore formal and direct. The keywords in scientific communication is precision and transparency. As a cause of this, the language spoken and written by scientists is formal. Scientists try to be as precise as possible, so that the publications cannot be misunderstood. This precision is for example obtained through mathematics and physics.

The use of the scientific langauge is for a student the most important part, maybe even more important than the collected data. The formulation of this report will illustrate the strategy of how the work is done so that every single bit can be analyzed both as a separated part and in unity with the context. Therefore this report will aim at using the precise scientific language and describing expressions quantitatively and exact rather than using everyday imprecise terms such as “good”, “bad”, “many” or “useful”. Furthermore it will aim to use a schematically and illustrative presentation rather than a “text only” presentation. A part of the report not included under these rules is the discussion where there is left room for estimations. [Føllesdal et al., 1995]

3.4 Critical assessment

When working with objects on the nanoscale it is important to be aware about the accuracy and credibility of the instruments in use. As a consequence of the nature of nanotechnology it is impossible to gain relevant knowledge about nanoscale objects without proper instruments. This entails a number of demands to the measuring instruments, and it assumes that one has to be critical about the results gained before using them in scientific publications. In the light of this the concepts of validity and reliability are introduced to help evaluate the instruments and data composed by them in a critical assessment.

Validity

The validity of an experiment is on the overall a discussion about whether what is measured is what is intended to be measured. For this purpose different conditions are reviewed, including the stringency and the accuracy of the experiment, for example in relation to the design of the experiment and a consideration about what was measured and what was not. Also, validity concerns about whether alternative explanations of the results are discussed.

A given experiment can be evaluated in different steps. At the first step a hypothesis is applied to the experiment. Is this a reasonable way to gain the information the scientist are attempting to obtain? Is it well designed? Does the experiment seem to work reliably? The next step is to try to compare the test with another similar one, in order to verify the accuracy and thereby the validity. Comparing the test with the theory in order to obtain an agreement between the two is the next step. To achieve validity one must first specify the theory and examine the empirical measurements, and then interpret and compare the empirical results with the theory in order to verify the achieved result. The last objective is to discuss to which extent the specific measurement scopes the whole specter being measured. In order to achieve an acceptable validity, it is important to construct the experiment so that all significant sources of errors are being addressed [writing.colostate.edu, 2004].

Reliability

In order to utilize the results of a scientific experiment it is important that one can trust that the obtained results do reflect reality. This is where the concept of reliability comes into play. In an overall view, reliability is a measure of the extent to which the obtained results can be used scientifically. Two important ways of achieving reliability is to repeat the test, and to do parallel testing with other similar measuring techniques.

For example, executing the same experiment multiple times enhances the reliability of the test. By performing the same test several times with a time interval, and then comparing the results, gives knowledge about the stability of the test and the measuring instruments. The atomic watch in Frankfurt can be used as an example. If a watch is calibrated in accordance with this and then compared one month later, the calibrated watch will most likely display a different time than the Frankfurt watch. By replicating this test a number of times, a measure of the stability of the watch is made.

Another factor which is of great importance, is the difference between the spectators involved in the experiment. The obtained results might be interpreted differently by different spectators, and this issue needs to be addressed too. This is also a part of the reliability of the results. [writing.colostate.edu, 2004].

Chapter 4

Materials and Methods

4.1 Separation of CNT Bundles

In this section the separation of the CNTs in the solution by use of SDS, centrifuge and ultrasound is described. Each section serves to describe a part of the separation process.

Solution

In Table 4.1 the chemicals used to produce the the 1 wt % SDS solution are depicted. The chemicals are mixed in a reaction tube and afterwards put into a mortar. The mortar is used to destroy the unoccupied micelles of SDS formed in the mixing process and to separate the bundles by shear forces to make room for the SDS. After the mortar treatment, the solution is placed in another reaction tube covered in ice to prevent heating and boiling while the solution is sonicated. The sonication is done to separate the remaining bundles. Now the solution is set for the centrifuge.

Chemical	Mass
D_2O	$5g$
SDS	$50mg$
CNT	$5mg$

Table 4.1: The chemicals and the amount of these used in the experiment

Coating

The purpose of coating is to prevent the molecular interaction between two substances. In analysis of CNTs coating plays an important role. Coating of CNTs prevents the tubes from forming bundles, and depending on the coating substance, they can be made soluble in water or another substance. Sodium dodecyl sulfate, or SDS for short, has proven to be a suitable surfactant because it impedes formation

of bundles and makes CNTs soluble in water. The SDS molecule has a chain of 12 carbon atoms, attached to a sulphate group. See Figure 4.1.

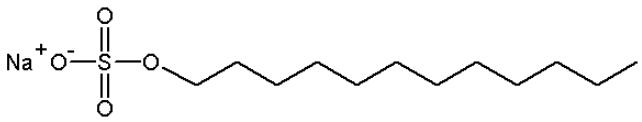

Figure 4.1: A model of the SDS molecule. When dissolved in water it is ionized in sodium and dodecyl sulfate.

When the SDS molecules are dissolved in water it dissolves into the ions, sodium and dodecyl sulfate. The decomposition makes the SDS molecules amphiphilic. The carbon end is hydrophobic and the ionized end becomes hydrophilic. This amphiphilic property forces the SDS molecules to make formations where the hydrophobic groups are placed in the center and the hydrophilic groups on the surface of the formation. This formation is called a micelle and it is the reason why the SDS molecules remain soluble in water. It is this ability to form micelles, that is utilized with CNTs.

When CNTs and SDS are mixed in D_2O the hydrophobic group of SDS will be adsorbed by the surface of the CNTs. This adsorption creates micelles around the CNTs, which makes them soluble in water. Furthermore the negative charges on the surface of the micelles prevent aggregation of the CNTs [wikipedia.org, 2005].

Different models for the organization of SDS molecules on the CNT surface have been suggested. The SDS molecules can be oriented perpendicular to the surface of the CNTs and thereby forming a monolayer. Figure 4.2 shows how the SDS molecules are attached to the surface. Two other suggested arrangements are based on previous studies of molecular organizations of surfactants at the solid-liquid interface. In these cases the SDS molecules formed half-cylinders on the surface of the graphene layer, and because CNTs are made of rolled-up graphite sheets, the SDS molecules may also form half-cylinders on the surface of the CNTs. The half-cylinders can be orientated parallel or perpendicularly to the tube axis. The orientations are illustrated in Figure 4.2. [Cyrille, 2005]

TEM pictures of SDS coated CNTs have shown half-cylinder orientation perpendicular to the tube axis, forming rings around the tube. In some cases the half-cylinders were tilted 2 to 30° in proportion to the tubes axis, which may indicate formation of right or left helices or double helices. It has been suggested that this tilting could be caused by the graphite network in the tube, but it has not yet been proved [Cyrille, 2005].

Centrifuge

A centrifuge is an instrument capable of accelerating a solution or a substance into an circular motion in order to filter off undesired particles from the solution.

By applying a centrifugal force, the different particles in the solution will be spread. Because the force needed to accelerate the particles is proportional to the

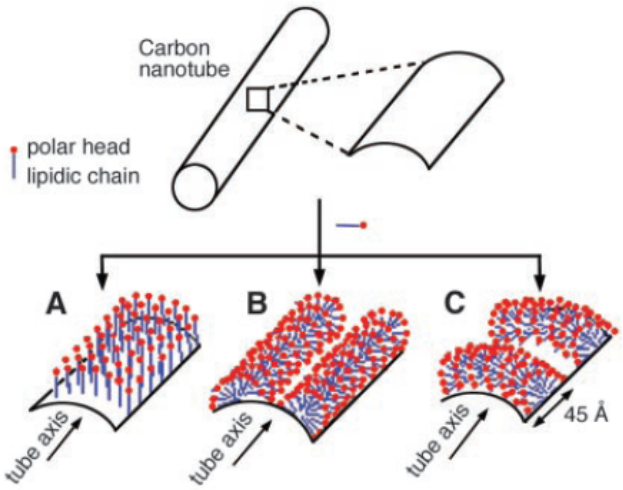

Figure 4.2: Different possible organization of SDS molecules on the surface of CNTs. ***A*** *The molecules could be absorbed perpendicular to the surface, forming a monolayer.* ***B*** *The SDS molecules could be organized into half-cylinder orientated parallel to the tube axis.* ***C*** *The SDS molecules cold form half-cylinder perpendicular to the tube axis.*
[Cyrille, 2005]

mass, particles with high density will have a tendency to be drawn towards the outskirts of the solution, leaving the lighter particles closer to the center. This is utilized to separate individual separated CNTs from SDS micelles, aggregated CNTs and metal particles. Individual CNTs encased in a close-packed SDS micelle have a density at about $\rho = 1.0\frac{g}{cm^3}$ while D_2O has $\rho = 1.1\frac{g}{cm^3}$. On the other hand, CNTs bounded together have an approximated gravity at $\rho = 1.2\frac{g}{cm^3}$ or higher. In addition, eventual excess metal particles from the synthesis have a density at about $\rho = 2.0 - 3.0\frac{g}{cm^3}$. This entails that the supernatant can be decanted from the solution, leaving the CNT bundles and metal particles. [O'Connell et al., 2002]

The data from the centrifuge are shown in Table 4.2

Parameter	Value
$Radius$	$14.3cm$
$Velocity$	$10000rpm$
$Duration$	$20minutes$
$Acceleration$	$16000g$

Table 4.2: The data of the ultracentrifuge used in the experiment.

Ultrasound

Ultrasound is sound pulses with a frequency higher than the upper limit of the human hearing, approximately 20 kilohertz [wikipedia.org, 2005]. Because the frequency is high the energy of the waves is high. This enables the use of ultrasound in the destruction of clusters of CNTs. The high energy of the ultrasound is powerful enough to overcome the van der Waals forces between the CNTs. This makes room for SDS to be attached to the surface of CNTs. The energy of the ultrasound can make the solution boil. This is prevented by placing the sample in ice and setting the ultrasound on pulsating mode instead of continuous. [wikipedia.org, 2005]

The ultrasound is generated by applying a AC-voltage to a piezo crystal. This type of crystal has the ability to change its volume under the influence of an alternating electric current. This change of volume sets the air around the crystal in motion and this creates the ultrasound. In a solution the ultrasound will form and implode bubbles with such a speed that the temperatures can reach $5000°C$ locally. The extend of these local temperatures are in the size of micrometers. Therefore this will only affect the overall temperature in the solution to such an extent that it is possible to keep the overall temperature constant by placing the solution in ice. [www.britannica.com, 2005]

The instrument which will be used is a UP 200S Ultraschallprozessor.

4.2 Spectroscopy and Microscopy

In this section the experiments performed on the CNTs will be presented. Also, a number of formulas and methods utilized with the experiment results will be introduced. The experiments which have been conducted are absorbance spectroscopy, fluorescence spectroscopy, Fourier transform infrared spectroscopy, Raman spectroscopy, atomic force microscopy and scanning electron microscopy.

Absorbance Spectroscopy

Absorbance spectroscopy is used to determine at which wavelength a solution absorbs light. The solution is placed in a cuvette and light is sent through the solution. When the wavelength are changed over time and the different intensities are recorded, the absorption spectrum can be drawn. The data collected is an expression of the optical properties of the solution.

It is possible to calculate the placement of the peak if the diameters and chiral angels are known for the CNTs. Equation 4.1 is suitable for calculation of those peaks.

$$\overline{\nu}_{Abs} = \frac{10^7 cm^{-1} nm}{145.6nm + 575.5 \cdot d} + \frac{A \cdot \cos(3 \cdot \alpha)}{d^2} \tag{4.1}$$

$\overline{\nu}_{Abs}$ is photon frequency in cm^{-1}. A is equal to $1375 cm^{-1} nm^2$ for $(n-m) mod 3 = 1$ or $-1475 cm^{-1} nm^2$ for $(n-m) mod 3 = 2$. α is the chiral angle and d is the diameter

of the CNT [Bachilo et al., 2002].

In this case diameters and chiral angles of the CNTs are unknown and therefore Equation 4.1 will not be used to calculate the placement of the peaks in the absorption spectrum. Instead Equation 4.1 will be used to calculate diameters and chiral angles. When the equation is used in this way a problem occurs because the equation now have two unknown factors. This problem can be solved by utilizing the fact that CNTs fluoresces. This means each emission peak will have a corresponding absorption peak. The emission peak can be calculated with Equation 4.2. Therefore when the absorption spectrum and the corresponding emission spectrum have been measured it is possible to set up two equations with two unknown factors for each absorption emission pair and thereby calculate diameters and chiral angles. The diameters and chiral angles can be used to determine the (n, m) integers.

In this experiment a cuvette will be filled with CNTs in a $1\%SDS$ solution and afterwards placed in an absorption spectrophotometer. The absorption will be measured from $300nm$ to $1700nm$. Because the detectors cannot detect such a wide spectrum, two different detectors running from respectively $300nm$ to $1000nm$ and from $900nm$ to $1700nm$ are used.

The spectrophotometer which will be used is Ultrospec 2000 from Pharmacia Biotech. More information about absorbance spectroscopy can be found in Appendix A.

Fluorescence Spectroscopy

CNTs are build from carbon atoms placed in an aromatic system. This type of system have a tendency to fluoresce when they are exposed to light with the proper wavelength. The light excites electrons from the ground state to a higher energy level where they will undergo a radiationless transition to a lower metastable state. From this lower metastable state the electrons will return to the ground state by emission of a photon. The wavelength of the photon will be longer than the wavelength of the exciting photon. Fluorescence spectroscopy can be used to draw an emission spectrum, where the peaks illustrates the emitted wavelengths. In connection with CNTs is also possible to calculate where the peaks will occur in the spectrum using Equation 4.2.

$$\overline{\nu}_{Em} = \frac{10^7 cm^{-1} nm}{157.5nm + 1066.9 \cdot d} + \frac{B \cdot \cos(3 \cdot \alpha)}{d^2} \tag{4.2}$$

$\overline{\nu}_{Em}$ is photon frequency in cm^{-1}. B is equal to $-710 cm^{-1} nm^2$ for $(n-m) mod 3 = 1$ or $396 cm^{-1} nm^2$ for $(n-m) mod 3 = 2$. α is the chiral angle and d is the diameter of the CNT [Bachilo et al., 2002].

In this experiment a cuvette is filled with CNTs in a $1\%SDS$ solution and afterwards placed in a fluorescence spectrophotometer. The fluorescence spectrophotometer is set to expose the solution with a specific wavelength of light and afterwards detect the emission. The experiment is repeated with different wavelengths of the

light The chosen wavelengths are those wavelengths that creates peaks in the absorption spectrum. In this way it is possible to determine each absorption/emission pair. After the absorption/emission pair has been found, the diameter and chiral angle can be calculated with Equation 4.1 and Equation 4.2. When the diameter and chirality are known, it is possible to calculate the (n, m) integers. When the emission is not known the formulas Equation 4.2 and Equation 4.1 cannot be used. Instead a table which describes the relation between absorbance and (n, m) vectors can be used. This table is found in [Bachilo et al., 2002]. The fluorescence apparatus used in this experiment is a Version 4 FS PTI Beta Build 00091. More information about fluorescence spectroscopy can be found in Appendix B.

Fourier Transform Infrared Spectroscopy

FTIR can be used to observe which wavenumber correspond to the vibrations of the molecular bonds. These wavenumber will be shown as peaks in the absorption spectrum between 800 and $4000cm^{-1}$. The peaks in the spectrum will be compared to data from IR Wizard [uni potsdam.de, 2005] and interpreted. IR Wizard is a database developed by the University Potsdam, which contains information about characteristic IR band positions. When using this method it is important to have an idea of which molecules the solution contains, as one specific wavenumber may correspond to different bonds.

CNTs in a $1\%SDS$ solution is placed on the transparent crystal of the instrument and IR light is sent through the crystal. It is thereafter reflected by the solution and is again passed through the crystal to the detector. The spectrum is drawn from the light intensity.

It is important to make a measure without the solution containing the subject being examined, in this case CNTs. This calibration is done in order to be able to determine which peaks occurs from the solution (SDS and D_2O) and which occurs from CNTs.

The following FTIR instrument will be used; Producer: Oriel Corporation. Light source: Model 60100. Monochromator: Model 77200. For more information about Fourier Transform infrared spectroscopy see Appendix C.

Raman Spectroscopy

In Raman spectroscopy Raman scattering of light is utilized to produce a Raman spectrum of the sample. When incident light hits the sample the light it scattered. Most of the incident light is scattered at the same wavelength, but a certain fraction of the light interacts with the molecules of the sample, and is scattered at a different wavelength which can be either higher or lower than the incident wavelength.

The peaks in the Raman spectrum of CNTs gives information about the diameter distribution and metallic character of the CNTs. These properties can be determined from the placement of the peaks.

Scan	Type	Subject	λ_{focus}	Exposure time	Repetitions
1-2	Extended	CNT	-	60 s	2
3	Extended	SDS	-	60 s	1
4-7	Static	CNT	350 cm^{-1}	240 s	4
8-9	Static	CNT	1600 cm^{-1}	60 s	2
10-11	Static	CNT	1600 cm^{-1}	30 s	2
12	Extended	CNT Raw	-	10 s	1
13	Static	CNT Raw	350 cm^{-1}	10 s	2
14	Static	CNT Raw	1600 cm^{-1}	10 s	2

Table 4.3: The parameters of the different scans.

The diameter is inversely proportional to the Raman frequency of the RBM peak, and the proportionality factor is equal to $248cm^{-1}nm$. Therefore the diameter can be calculated from the formula:

$$\omega_{RMB} = \frac{248cm^{-1}nm}{d_t} \tag{4.3}$$

Here ω_{RBM} is the wavenumber of RBM peak, and d_t is the diameter of the CNT. The conducting or semiconducting properties of the CNTs can be calculated from the G^- and G^+ peaks by using Equation 4.4, where ω_G^- and ω_G^+ are the Raman frequencies corresponding to the G^- and G^+ peak. β is $47.7cm^{-1}nm^2$ for metallic CNTs and $79.5cm^{-1}nm^2$ for semiconducting CNTs. d_t is the diameter of the CNT [Dresselhaus et al., 2002]

$$\omega_G^- = \omega_G^+ - \frac{\beta}{d_t^2} \tag{4.4}$$

In order to prepare the solution for the Raman spectroscopy it will be sonicated at 200W before it is placed in the instrument. This will be done to destroy aggregations of CNTs in the solution. After the sonication a few drops of the solution will be put on a slice and heated in a furnace to vaporize the water. The slice was put into the Raman spectrophotometer and the laser was focused at the center of the drop, where the density of CNTs is expected to be highest.

The laser of the raman spectroscopy device was a HeNe laser at a wavelength of 633 nm, corresponding to an energy of 1.96 eV, with a magnification of 50x. The intensity of the laser is set to 50%. The Raman spectroscopy used was an Renishaw inVia Raman Microscope. The various scans are listed in Table 4.3. For more information about Raman spectroscopy see Appendix D.

Atomic Force Microscopy

The AFM works by dragging a tip, mounted on a cantilever, over the sample and thereby measuring the topography. The position of the tip can be controlled with

high precision so it is possible to examine regions in micro- and nanometer scale, thus making it possible to examine crystals or small areas of a surface.

AFM will be used to examine if any single CNTs are separated from the bundle.

CNTs in a 1%SDS solution will be placed on a siliciumwafer and dried. The wafer will then be examined in the AFM. The AFM is a Nanosurf Easyscan E-Line. See Appendix E for more information.

Scanning Electron Microscopy

Scanning electron microscopy uses a beam of electrons to scan a surface. The electrons can be accelerated using their charge to achieve a wavelength much shorter than that of visible light or even x-rays. This results in a resolution that by far exceeds that of optical microscopes. The SEM scan takes place in vacuum so that particles from the air do not interfere with the electron stream. The SEM scan can be used to determine if the CNTs has been separated. For a more detailed description of the SEM instrument see Appendix F

In order to determine if the CNTs has been separated some of the tubes must be fixated on a silicon wafer. This is done by placing a drop of the CNT solution on the wafer. Afterward the wafer is heated in order to vaporize off the D_2O and prevent contamination by unwanted particles. When the sample is dried it is placed in the SEM instrument. The instrument used was an LEO 1550 SEM.

Chapter 5

Results

5.1 Absorbance Spectroscopy

Absorbance spectroscopy measures the light absorbed by a substance. The output is a data stream that can be plotted in an x, y coordinate system. The wavelength is plotted in the direction of the x-axis and the intensity in the direction of the y-axis.

The results from the absorbance spectroscopy experiment can be used to determine the composition of CNTs in the solution, by providing information about the distributions of the (n, m) integers. [Bachilo et al., 2002]

$\lambda_{Peak}(nm)$	$Tolerance$	λ_{Table}	$Assignment$	$Diameter(nm)$	$Conduct.$
561	± 10	551/567	$(9,2)/(6,5)$	0.8/0.8	*Semi*
598	± 10	587	$(8,4)$	0.83	*Semi*
651	± 5	644/647	$(7,5)/(7,6)$	0.8/0.9	*Semi*
734	± 5	728/734	$(8,7)/(10,2)$	1.0/0.9	*Semi*
785	± 5	786/790	$(10,5)/(9,7)$	1.0/1.1	*Semi*
942	–	–	–	–	–
1137	–	–	–	–	–

Table 5.1: The λ_{peaks} found in Figure 5.1 and Figure 5.2 compared to λ_{Table} - the table found in [Bachilo et al., 2002]. The (n, m) structures has been determined from these data and the diameters are calculated from Equation 2.1. All assignments are found to be semiconducting.

The peaks on the absorbtion curve from Figure 5.1 and Figure 5.2 were analyzed and the approximated wavelength of the peaks was determined. The bulk numeric results were then analyzed, and the specific wavelengths of the peaks could be determined.

The absorbance spectrum of D_2O and SDS was measured from 300-1700 nm. From 300-1000 nm there was no absorbance and therefore this has not been shown on the graphs. From 900-1700 nm SDS absorbs light and this is shown in Figure 5.2

Comparing these results to the table in [Bachilo et al., 2002] indicates that the

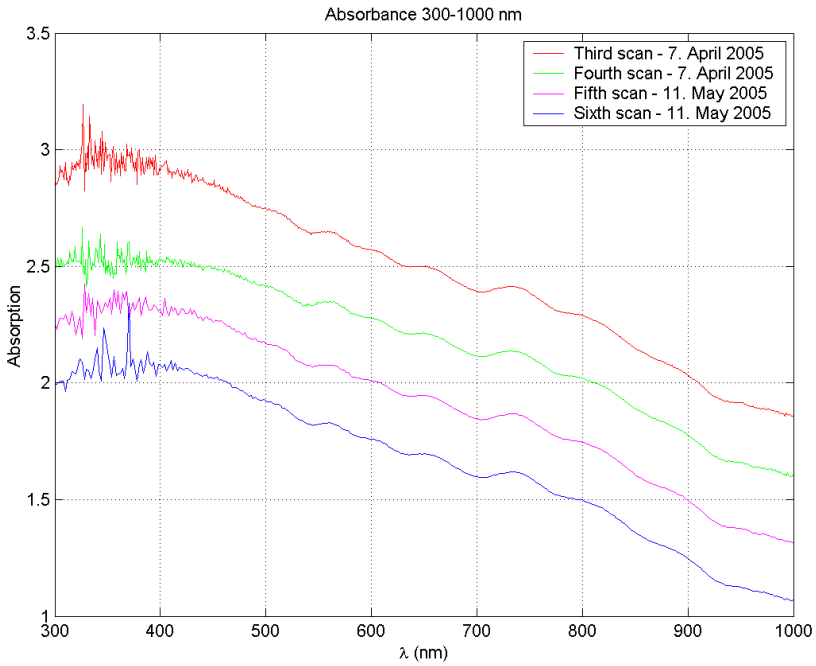

Figure 5.1: The curves obtained from the absorbance spectroscopy experiment between $300nm$ *and* $1000nm$ *are shown with an offset. The peaks on the graph were measured and can be found in Table 5.1*

.

CNT composition consists of the assignments shown in Table 5.1. Equation 4.1 and Equation 4.2 has not been used to calculate the (n, m) integers because no useful fluorescence data was obtained. The peaks at $\sim 942nm$ and $\sim 1137nm$ can not be compared to the table from [Bachilo et al., 2002] as the table only contains wavelengths up to $928nm$. The diameter is calculated from Equation 2.1. The assignment is furthermore presented in Figure 5.3.

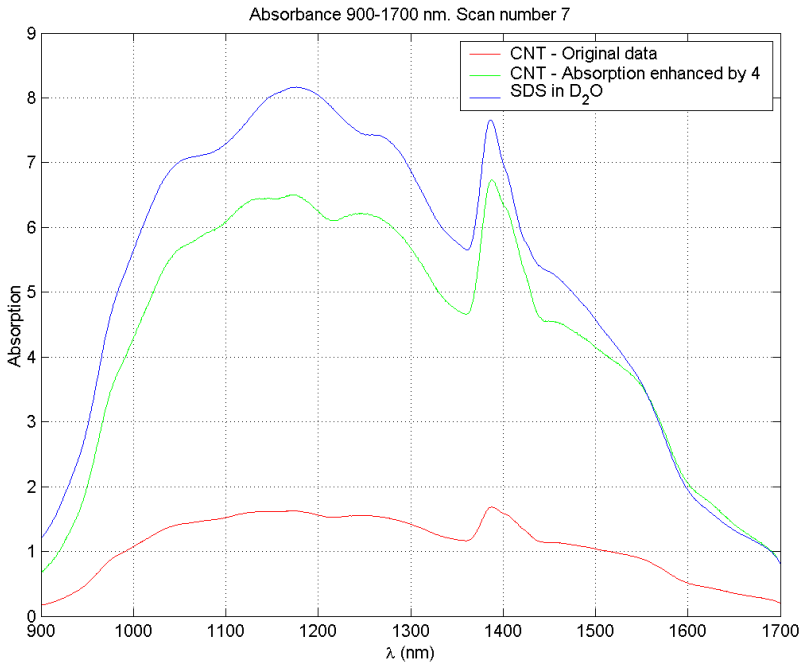

Figure 5.2: The curves obtained from our absorbance spectroscopy experiment between $900nm$ *and* $1700nm$*. The only peak on the CNT graph that does not appear on the SDS curve was measured and can be found in Table 5.1.*

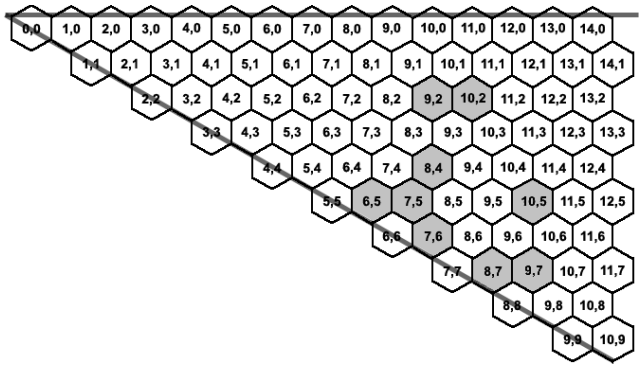

Figure 5.3: The (n,m) structure found by the peaks in the absorbance spectroscopy.

5.2 Fluorescence Spectroscopy

Fluorescence spectroscopy is used to determine if a materiel has fluorescent properties and where the emission takes place. The output is a data stream that can be plotted in an x, y coordinate system. The wavelength is plotted in the direction of the x-axis and the intensity in the direction of the y-axis.

Fluorescence spectroscopy was conducted in order to examine the respective wavelengths of emission for each excitation wavelength. This was done to determine the distribution of CNTs (n,m) indices according to the article of [Bachilo et al., 2002] and Equation 4.2. It was however not possible to achieve any spectra with clear emissions peaks. One of the spectra is shown in Figure 5.4, where $530nm$ was used as the excitation wavelength. As it can be seen in the spectrum a peak occur around $530nm$ which is caused by Rayleigh scattering.

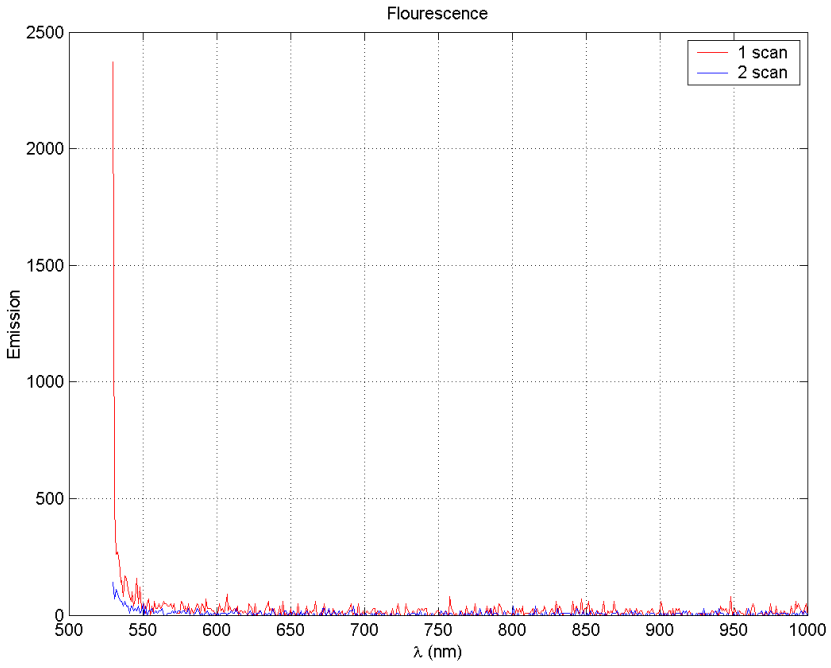

Figure 5.4: A fluorescence spectrum of CNTs in a 1% SDS solution. The excitation wavelength was $530nm$

5.3 Fourier Transform Infrared Spectroscopy

The results from infrared spectroscopy can be used to determine which types of bonds are present in the solution. From the graph on Figure 5.5 the results from infrared spectroscopy can be seen.By comparing the data on Figure 5.5 with data

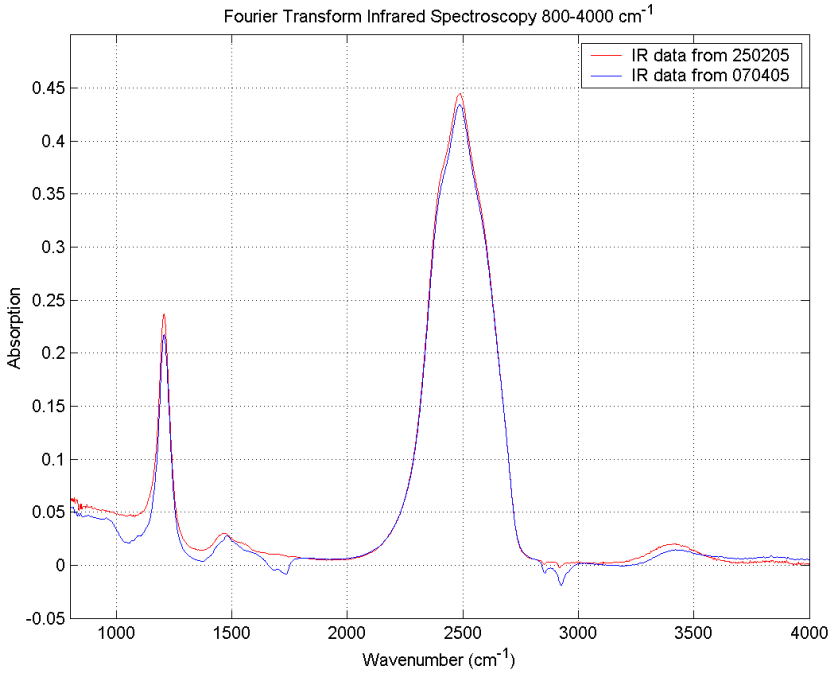

Figure 5.5: This graph shows the results from infrared spectroscopy. The peaks are labeled on the graph. The first peak at $1200cm^{-1}$ *indicates SDS. The next peak at* $1450cm^{-1}$ *indicates CNT. Peak 3 at* $2500cm^{-1}$ *indicates* D_2O *and the last peak at* $3400cm^{-1}$ *indicates water.*

from the IR Wizard [uni potsdam.de, 2005], information on the types of bonds in the sample can be found. The results can be seen in Table 5.2.

Wavenumber	Bond	Molecule
1200 cm^{-1}	C-H / C-O	SDS
1450 cm^{-1}	aromatic system / $C = C$	CNT
2500 cm^{-1}	D-O	D_2O
3400 cm^{-1}	O-H	H_2O

Table 5.2: The different bonds in the sample are shown.

5.4 Raman Spectroscopy

Raman spectroscopy has become closely connected with CNTs due to the resonance quantum effect. From this effect the peaks on the raman spectrum will be evident compared to raman spectroscopy on e.g. graphite.

In Figure 5.6 the full range of the raman scan of CNT is displayed. The radial breathing mode (RBM) peaks are between 100 and 400 cm^{-1}, the D-band can be seen between 1250 and 1450 cm^{-1} and the G-band is from 1500 to 1700 cm^{-1}. The intensive peak around 2600 cm^{-1} corresponds to the harmonic from the small peak at 1300 cm^{-1}. Peaks are seen at 1740, 1915, 2875, 2430 cm^{-1} and in the range from 500 to 1000 cm^{-1}. Some of these might be harmonics and others might be caused by SDS.

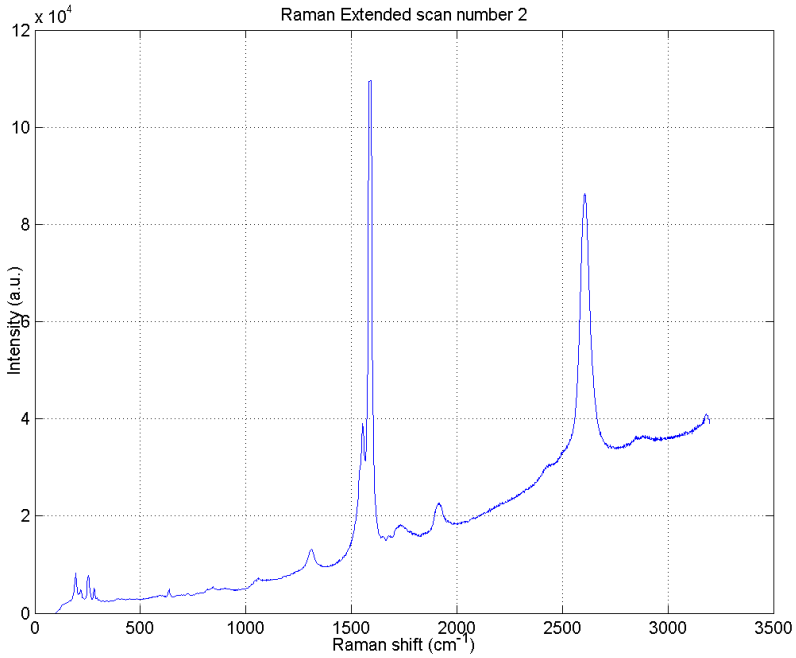

Figure 5.6: An extended raman scan. RBM, D-band and G-band peaks are observed at 100-400 cm^{-1}, 1250-1450 cm^{-1} and 1500-1700 cm^{-1} respectively. Furthermore some harmonics and additional peaks are observed. The slope of the curve is accounted by SDS, see Figure 5.7.

The extended SDS graph, can be seen in Figure 5.7. The slope of the graph is clearly seen and at the same scale as in Figure 5.6. Therefore the slope of the raman spectrum of the CNTs can be accounted for by SDS. Evident peaks are observed at 1100 and at 2800 cm^{-1} each corresponding to a peak in Figure 5.6.

Furthermore an extended scan of the raw CNTs were conducted. See Figure 5.8. The location of the peaks are generally at the same Raman frequency as in Figure

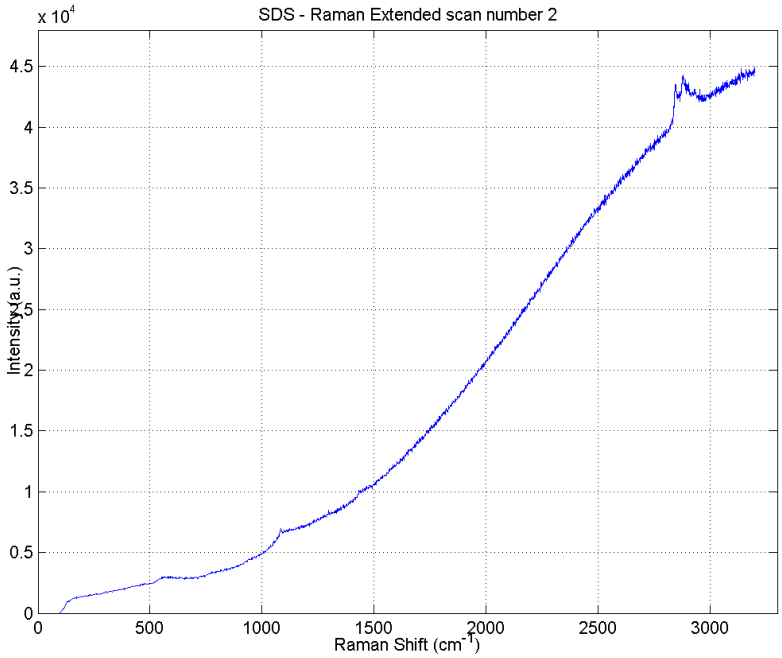

Figure 5.7: The raman spectrum of SDS in D_2O. Note that this graph explains some of the undetermined peaks found in Figure 5.6.

5.6.

Figure 5.9 and Figure 5.10 shows static scans of the RBM and G-band.

The Raman frequency of the peaks from the static RBM scan are shown in Table 5.3 with the diameters calculated by Equation 4.3.

RBM #	peak value	d_t
1	159.5 cm^{-1}	1.6 nm
2	164.0 cm^{-1}	1.5 nm
3	195.5 cm^{-1}	1.3 nm
4	218.0 cm^{-1}	1.1 nm
5	254.5 cm^{-1}	1.0 nm
6	282.5 cm^{-1}	0.9 nm
7	296.5 cm^{-1}	0.8 nm

Table 5.3: RBM peaks and the calculated respective diameters.

The G^+ peak is at 1589 cm^{-1} and the broad G^{-1} band is between 1540 and 1560 cm^{-1}.

The ratio between the intensity of the G^+ peak and the G^- peak is proportional to the ratio between the conducting and semi-conducting CNTs [Kukovecz et al., 2002]. The different intensities of the two peaks and the corresponding relations are listed

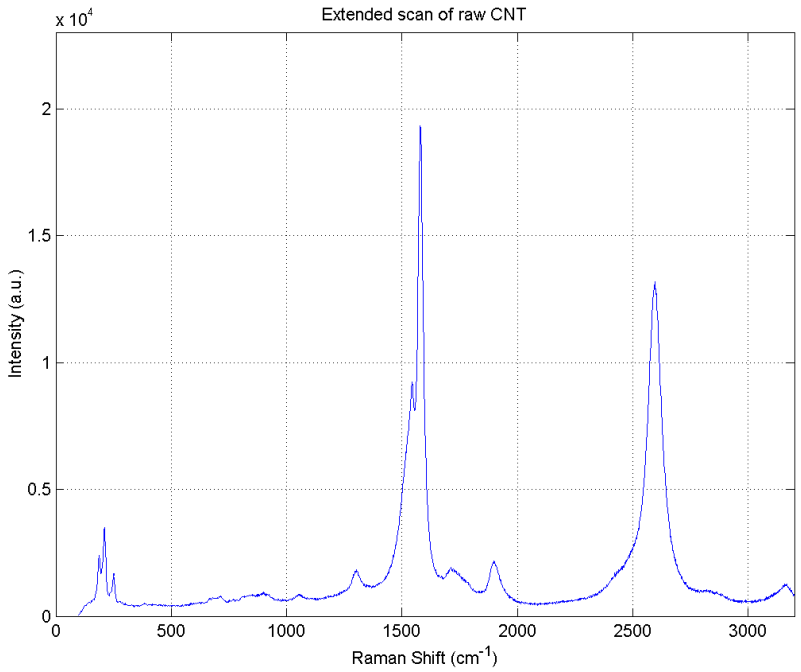

Figure 5.8: The raman spectrum of the raw untreated CNT. Notice the flat slope and the less intensive peaks compared to Figure 5.6.

in Table 5.4. This results in an average giving 33.5% metallic CNTs with a tolerance of 5.68% if the bundled CNTs are left out and 41.0% in with a tolerance of 0.165 with both bundled and separated CNTs.

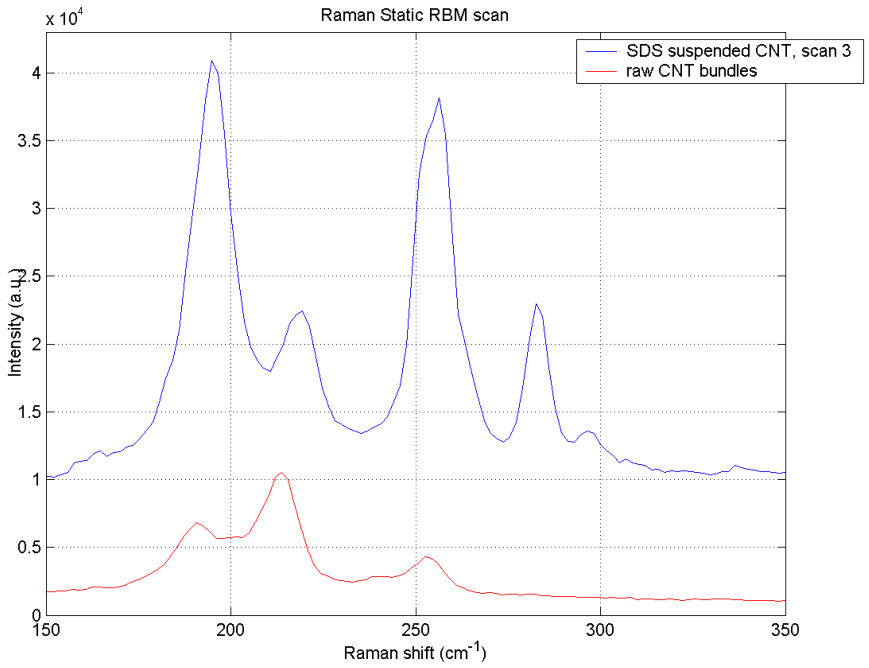

Figure 5.9: Static RBM Raman scan of both the SDS suspended CNT and the raw bundled CNT.

	Scan number	G^- in a.u.	G^+ in a.u.	$\frac{G^-}{G^+}$
with SDS	1	1.64	3.66	0.488
	2	2.43	7.56	0.321
	3	1.99	6.95	0.286
	4	2.2	7.75	0.284
Raw Tubes	1	0.96	2.03	0.474
	2	2.65	4.87	0.544

Table 5.4: The different intensities of the G^- and G^+ along with the corresponding relations.

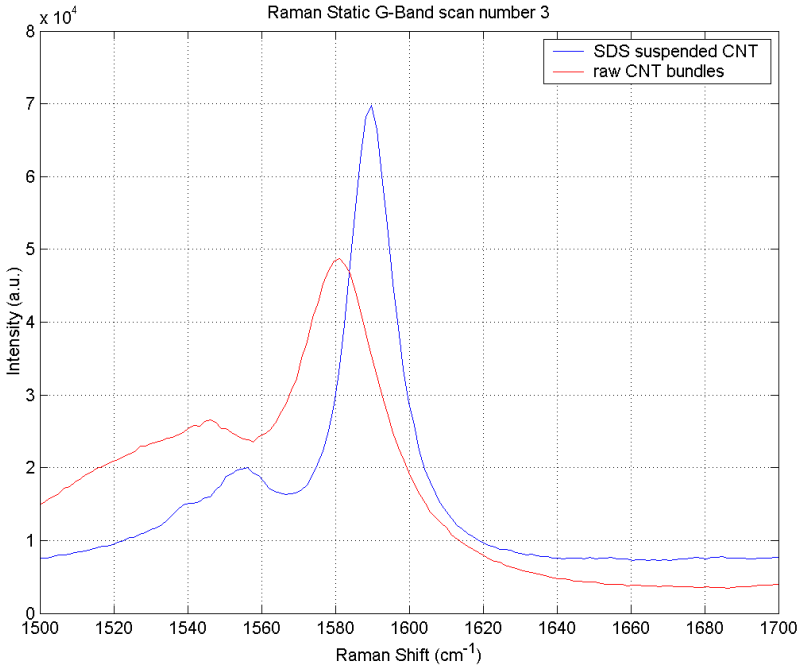

Figure 5.10: Static G-band Raman scan of the SDS suspended CNT and raw bundled CNT.

5.5 Atomic Force Microscopy

The purpose of AFM is to get a typographic image of the CNTs. Figure 5.11 shows one of the scans made with Nanosurf easyScan. As it appears on the symbol line in the right side of both images, darker color means lower contour.

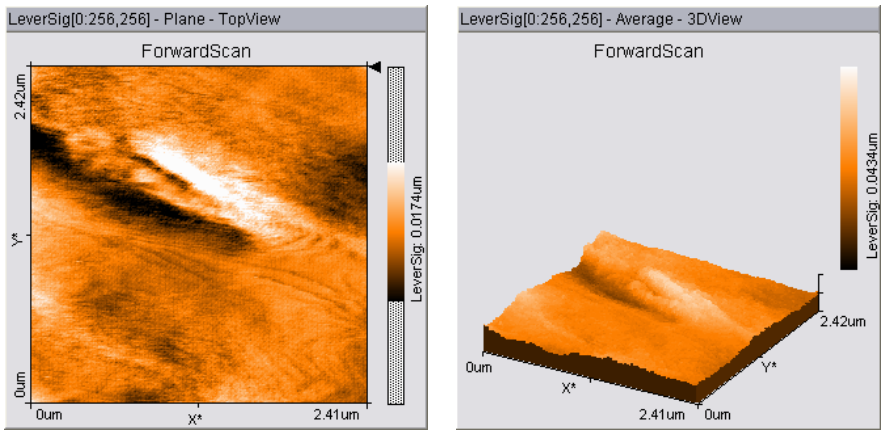

(a) (b)

Figure 5.11: The obtained AFM scan. (a) shows a 2D view of the data, and (b) shows a 3D view.

None of the obtained pictures with images of structures could be identified as tubes or clusters of tubes. The indistinct results may be the result of a calibration error in the AFM instrument. This may have caused the needle to not be in sufficient contact with the sample. Hence it was not possible to obtain usable results using the AFM.

5.6 Scanning Electron Microscopy

The purpose of the SEM experiment was to verify if the CNTs was separated or in bundles. The pictures in Figure 5.12 show that the CNTs are placed in bundles on the silicon wafer. This will be further discussed in Section 6.6. The structure in the picture (a) is SDS crystals formed by the evaporation process. The other pictures show clusters of CNT bundles. The magnification of the pictures is between 5000 and 40000.

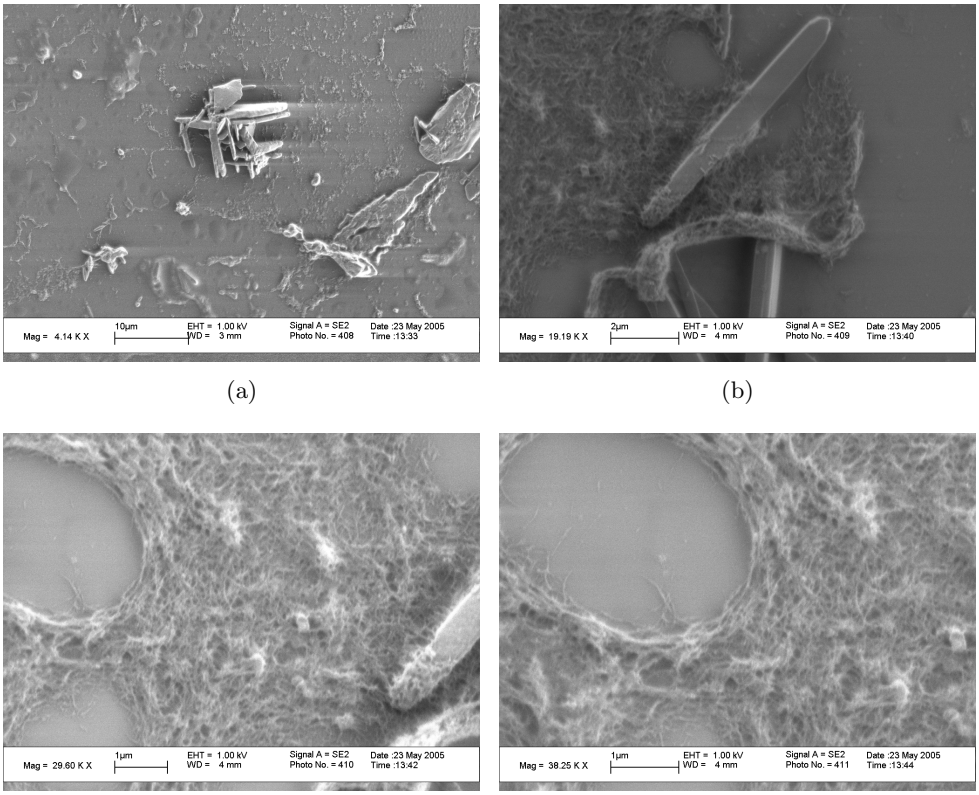

(a) (b)

(c) (d)

Figure 5.12: 4 SEM pictures of CNT at different magnifications. (a) is magnified by ~ 5.000 *and shows some SDS crystals. (b) is magnified by* ~ 20.000 *and shows CNT bundles around a crystal. (c) is magnified by* ~ 30.000 *and shows the CNT bundles in a area close to the one in (b). (d) is magnified by* ~ 40.000 *and shows a magnification of the left area in (c)*

Chapter 6

Evaluation and Discussion

A number of different methods was used to examine the solution of CNTs. An evaluation of the validity and reliability is made. In the AFM and fluorescence experiments the results showed to be dominated by noise and uncertainty, and this behavior will be explained.

Furthermore the results will be compared improve the description of the CNT distribution.

6.1 Absorbance Spectroscopy

The absorbtion analysis was conducted seven times. The first run was of no use because the concentration of CNTs in the sample was too high. Because of this an insufficient amount of light passed through the sample, and no useable spectrum with clear peaks was obtained. The solution to this problem was to add more D_2O. The amount of D_2O added was not measured, but this however, is not a problem for the outcome of the experiment. It is important is to have enough SDS fixated on the surface of the CNTs to keep them separated, and this is not changed when D_2O is added to the sample. If the concentration of CNTs in the sample is needed, or if an exact replication of the experiment was to be conducted, the amount of D_2O would be important.

The rest of the collected data was useful as a result of the dilution. In order to determine which influence SDS and D_2O had on the results an absorbance spectrum of SDS dissolved in D_2O was recorded. This showed that SDS and D_2O does not absorb light in the wavelength region between $300nm$ and $900nm$ but absorbs light between $900nm$ and $1500nm$. Hence, the peaks on the CNT curve in Figure 5.2 must be compared to the peaks on the curve showing the absorbance of SDS and D_2O. This implies that CNTs only absorbs light at $\sim 1137nm$ in the area between $900nm$ and $1500nm$.

The weak absorbance peaks can be explained mainly by three reasons. Firstly, the intensity of the light source could have been too weak. If the light source had been more powerful then more electrons would have been exited causing the peaks

to be more distinct. However, it is important to be aware of the point that if the light source had been too strong then it is possible that it could had damaged the sample. Secondly, the time of exposure on the sample could have been too short. If this been longer then more electrons would have been exited. In this case it was not possible to change the time of exposure. A third reason could be that there is a wide distribution of different CNT structures. This would cause a wide absorbance spectrum. This is likely because HiPCO produces a wide distribution of diameters.

The (n, m) assignments in Table 5.1 are based on results from [Bachilo et al., 2002] and as shown in Figure 5.3 the CNTs in the sample are all placed in the same area of the honeycomb. Furthermore the diameter of the CNTs are calculated from Equation 2.1 and the diameters come from Table 5.1. These diameters was calculated by using the table in [Bachilo et al., 2002]. This table was used because Equation 4.1 and Equation 4.2 could not be used because no useable emission data was obtained. The diameters were determined to be between $0.8nm$ and $1.1nm$ and this matches the data from the HiPCO production method, where the diameters are between $0.7nm$ and $2.4nm$. All (n, m) structures are found to be semi-conducting from Figure 2.4 in Section 2.4.

The peaks at 942 nm and 1137 nm was not listed in the table in [Bachilo et al., 2002] and therefore the (n, m) integers could not be determined from these peaks. If the (n, m) integers for these peaks could have been determined, both smaller and larger diameters might have been obtained.

The validity and reliability of the absorbance results is discussed in Section 6.7.

6.2 Fluorescence spectroscopy

The emission spectrum recorded shows that the CNTs do not fluoresce within the wavelengths measurable by the spectrophotometer. However, it is likely that the light source used to excite the sample was not powerful enough to produce observable fluorescence. The results from absorbance spectroscopy show weak absorbance peaks with an intensity of only 0.1 arbitrary units, and the fluorescence will be even weaker.

Fluorescence was measured up to $1000nm$ due to instrument limitations, but it is likely that fluorescence could be observed at wavelengths above $1000nm$. To enhance the emission signal, the time of exposure could have been longer. To do this the detector used to detect the emission would need accumulative properties. This could for example be achieved by using a CCD. In order to collect data from the region above $1000nm$ another detector must be used. It was planned to conduct an experiment with this detector, but due to time limitations it could not be made. If valid data from the fluorescence experiment had been obtained, Equation 4.1 and Equation 4.2 could have been used to characterize which types of CNTs are present in the solution.

6.3 Fourier Transform Infrared Spectroscopy

The results from IR spectroscopy is measurements of the vibrations of the bonds in the molecular structure of the CNTs, D_2O and SDS. As described in Section 2.4 the vibrations of these bonds is influenced by the molecules interacting with each other. Because of the many possible combinations of atoms the method does not give an exact answer to which bonds the peaks represent. One specific wavenumber may correspond to more than one type of bond. For example the peak at $3400cm^{-1}$ may correspond to both $O-H$, NH_2 and other molecular bonds. Therefore knowledge about the sample before conduction of the experiment is needed in order to make conclusions on the IR-results.

In the experiments conducted on the CNT solution it is expected to find $C-C$, $C=C$, $C-O$, $D-O$, $S-O$, $S=O$, $C-H$ bonds and aromatic systems. Analysis of the IR graphs with the archive from [uni potsdam.de, 2005] proves the presence of these bonds, except for $C-C$, $S-O$ and $S=O$ bonds. The $C-H$ bonds originates from SDS.

The $C=C$ bonds and aromatic systems in the solution are only found in the CNT honeycomb lattice, and therefore these bonds prove the presence of CNTs in the solution. The fact that CNTs are still found in the solution after centrifugation indicates a successful dissolution of CNTs by SDS coating in D_2O. Any unsuspended CNTs would have been filtered out in the centrifugation process along with graphitic remains. From these data a conclusion about the ratio of CNTs dissolved and the CNTs filtered off, cannot be made as there can be made no conclusion about the amount of CNTs in each micelle.

The largest peak in the spectrum is the peak at $2500cm^{-1}$ which originate from D_2O. This is expected because SDS and CNT is dissolved in D_2O. If the peak at $1200cm^{-1}$ originating from SDS is compared to the peak at $1450cm^{-1}$ it can be seen that the SDS peak is larger than the CNT peak by a factor of 8. This might be because 10 times more SDS than CNT was added to the solution.

In addition to the above listed bonds, $O-H$ bonds are present in the solution. This is because H_2O is present in the solution. Although H_2O was not added to the solution, it is added via the condensed water from the air.

6.4 Raman spectroscopy

From Raman spectroscopy it is possible to determine the diameter distribution and metallic character of the CNTs in the sample. Figure 5.6 shows an extended scan of the CNT sample. From this graph the RBM and G-band can be seen. In Figure 5.9 and Figure 5.10 a closeup of the RBM and G-band are shown. As it can be seen, multiple peaks in the RBM are obtained. This illustrates a distribution of diameters in the sample and not just a single diameter.

If Equation 4.3 is applied to the RBM frequencies, diameters between $0.9nm$ and $1.5nm$ are found. This is in agreement with the diameter distributions produced by

the HiPCO production method, which are in the range $0.7nm$ to $2.4nm$. Table 5.3 shows the calculated diameters and their respective wavenumbers.

Because only a single laser at $633nm$ was available, only those diameters which are Raman resonant at this wavelength shows peaks in the RBM area of the spectrum. To obtain information about those CNT diameters which does not show Raman resonance at $633nm$, it is necessary to use lasers with different wavelengths. Unfortunately these lasers were not available. Therefore CNTs with diameters other than those observed in our experiment may have been present in the solution.

The G-band in the Raman spectrum is dependant on the metallic character of the CNTs. In Figure 5.10 a closeup of the G-band is shown. By applying Equation 4.4, the distance between the G^- and G^+ peaks can be used to determine the metallic properties. This is however not appropriate because the tubes in the sample is a mixture of several different types of CNTs. Therefore the G^- and G^+ peaks will be based on an average of all the types of CNTs in the sample.

The G^- band shows dependance on the diameter of the tubes. By enlarging the G^- peak, several peaks show up. It was unknown if these peaks could be used to calculate the metallic character of individual diameters in the sample, and therefore this has not been done.

Table 5.4 shows the G^- and G^+ peaks and the ratio between them for both the raw CNTs and the SDS treated ones. The higher the ratio, the higher the concentration of metallic CNTs. Four static scans of the G-band were conducted, and as it can be seen from the table, the ratio vary from 0.284 to 0.488. The four scans were conducted at different spots on the sample, and this could explain the variety in ratios because the concentrations of semiconduction and metallic CNTs might vary across the sample. The raw CNTs show higher ratios than the SDS treated ones. The cause of this is not known.

By looking at Figure 5.8 and Figure 5.6 a major difference in intensity is seen. The raw CNTs show an intensity which is smaller than that of the SDS treated CNTs by a factor 5. This is because the exposure time between the two is different by a factor of 3 as can be seen in Table 4.3.

A second difference between the scan of the raw CNTs and the separated CNTs, is the absence of the peaks at $282cm^{-1}$ and $296cm^{-1}$ in the raw CNT scan. These peaks correspond to the smallest diameters of the separated CNT scan. It is not clear why these diameters are absent from the raw scans.

From the SDS scan it can be seen that those peaks which are relevant for CNTs are not influenced by SDS.

6.5 Atomic Force Microscopy

AFM-microscopy is a measuring method that uses a tip touching the surface of the sample, and results in a picture of the topography of the surface of the sample as output. Because of this, AFM is one of the most direct measuring instruments used in nanotechnology.

The results from our AFM experiment was as mentioned in Section 5.5 not usable. The collected data did not show the presence of CNTs. This could be due to the fact that the AFM microscope shortly after use was sent to the manufacturer for reparation. The need for reparation was also present under the conduction of the experiments.

The preparation of the silicon wafer is a likely source of error if the CNTs was not evenly distributed on the wafer then the reading of a specific area on the wafer could turn out as empty.

The most likely source of error in the AFM data was discovered using the method of Raman spectroscopy. While adjusting the focus of the instrument it was discovered that the SDS in the solution had formed crystals. This crystallization can be used to explain why the results from the AFM did not show signs of CNTs. In the case of Raman spectroscopy the drying process took place in an furnace, this meant that the drying process was fast and as a result of this the crystals formed was small. The slower drying process of the sample used in the AFM experiment (standard conditions) has probably formed crystals on the surface of the wafer. The bigger crystals raises the probability of making a reading directly on top of a crystal. This explains the smooth reading of the tip. The low contour read by the tip can be explained by two crystals lying next to each other or as a defect in the crystallization process. If the AFM microscope had returned from the manufacturer before the expiration of the project period, another attempt on collecting useful data would have been carried out. In this attempt the wafer should be prepared by using a furnace to vaporize the D_2O from the sample.

6.6 Scanning Electron Microscopy

SEM uses a beam of electrons that is reflected by the sample. The energy of the electrons used in SEM is high which gives a short wavelength. This makes it possible to obtain a high resolution.

The pictures gained through SEM showed that the bundles of CNTs was $30 - 50nm$ in diameter, which is small compared with the bundles of the raw tubes used as basis for the solution. It is difficult to determine the size of the raw bundles, but they can be estimated to be around $0.1mm$. This shows that separation has taken place in terms of a reduction of the bundle size. The reason why a higher magnification is not used, is because of bad conducting properties of the sample. If the conduction had been better it would prevent the buildup of static voltage. This would mean that the energy of the electrons used to analyze the sample could have been higher, thereby enhancing the resolution and contrast of the picture. The buildup of static voltage interfere with the electrons and changes their reflection by the sample thereby spoiling the contrast of the picture.

Even though the CNTs are coated with SDS they still form clusters due to van der Waals forces. Because of SDS this cluster formation will not happen until the polar environment of D_2O becomes super saturated. The result of this is that a

number of CNTs will end op in the same area. To prevent these cluster formations, the evaporation must be so fast that the CNTs do not move towards the center of the drop. This can either be done using a vacuum chamber, heating the wafer or letting the wafer stay untouched in a short period of time in order for some of the tubes to settle on the wafer, and then afterwards shake off the remaining water. Another method is to dilute the solution of the CNTs thereby reducing the concentration of the CNTs. Afterwards one of the evaporation methods can be used to remove the D_2O. This will make more room for the single CNT on the wafer.

6.7 Evaluation of quality

Spectroscopy is a general designation of different measuring methods utilizing the optical properties is the sample, and the absorbance or the emission is measured. This makes spectroscopy a non-direct measuring method, hence the results are evaluated using theories that by their nature may contain uncertainties. Also circumstances as the purity and the density of the solution may influence the results.

As we have performed a number of different spectroscopy measurements on the same subject, it can be said that we have attempted to achieve high reliability. In general, it is an interpretation of the theories that adds value to the results, and therefore the results are subjective.

Because our work has been based on articles which do not present any conclusions or clearly defined results, our spectroscopy experiments can be questioned.

Absorbance Spectroscopy

The absorbance spectroscopy was repeated a number of times and as the curves seemed similar the reliability was high. The validity of the (n, m) structure and diameter in Table 5.1 can be questionable as the results are determined by comparison to other results. Had these results been invalid, so would ours. The primary problem was that no absorbance/emission pair was obtained. Also, trying to determine the assignment and the diameter of the CNTs from the absorbance peaks resulted in some uncertainties. Because of the wide peaks on the graph, it was not possible to determine the exact wavenumbers, and therefore one peak could correspond to more than one (n, m) assignment and diameter. This puts a doubt on the validity of our experiments because there are alternate explanations for the same results. However, as the (n, m) assignments are placed close to each other in the honeycomb we consider the experiment successful.

Fluorescence spectroscopy

We obtained no fluorescence spectroscopy data, and therefore it is not possible to make a discussion of the validity and reliability of the experiment.

FTIR spectroscopy

For FTIR spectroscopy, the primary concern is the consideration about what is being measured and what is not, and the question about whether there could be alternative explanations to the results. In our experiments, however, the subject tested is well known, and the results obtained are acceptable. Moreover, the results seemed to be similar by doing repeated test, which can be used to describe the general validity and reliability as acceptable.

Raman spectroscopy

In Raman spectroscopy the graphs measuring SDS in D_2O, raw CNT and CNTs in SDS and D_2O were correlated and the results were plausible in relation to each other, hence the consider the reliability to be high. Also, performing similar tests on different locations on the sample resulted in similar graphs, and furthermore the results are reasonable in comparison with theoretical expectations, which lead us to the conclusion that the validity is high.

AFM

The AFM tip is very sensitive to external influences, which could cause the results to be invalid. Furthermore, the data obtained by AFM is limited to a distinct area of the subject, which we cannot presume to be representative for the hole sample. Also, the results are observed and interpreted, which causes the reliability to be low, as we do not know what we are looking at when viewing the output. Due to these conditions we have the opinion that the validity and reliability of the AFM is low. This is also reflected by our experiments.

AFM seems to be an instrument that can be used for visual presentation in order to make a report or paper more straightforward and easy to read. Also it can be used as a help to confirm hypothesizes, for example the question about whether our CNTs were separated. But it is difficult to make scientific conclusions on basis of AFM measurements.

SEM

The scanning electron microscope uses electrons to create an image of the topography of a sample, in more or less the same way as the optical microscope uses photons.

From SEM it is possible to determine if the CNTs are separated, because the pictures show structures with diameters below 50 nm. The SEM pictures shows what we expect to see, and therefore we believe that the results are valid.

6.8 Accumulative Discussion

The different experiments conducted each give information about the attempt on separating and characterizing the CNTs.

Through comparison of the IR and SEM experiments it can be seen that a certain amount of CNTs has been dissolved. This shows that the separation process was successful. The SEM scans shows partly separated longitudinal structures of 20-30nm in diameter and approximately 1 μm long. These structures are the SDS and CNT micelles with a center of CNTs covered with a layer of SDS. The depth of the SDS layer is not known but from the molecular structure of SDS a size in the area of 2 nm can be derived. The number of CNTs in each micelle can thereby not surpass 200 for a 20nm wide bundle from the diameters found in the absorbance and Raman spectroscopy experiments.

The diameters derived from the absorbance and Raman spectroscopy experiments are in consistency, showing diameters from 0.8 to 1.1 or 1.6 nm respectively. Absorbance spectroscopy does not show diameters above 1.1nm as data for comparison for absorbance peaks above 928nm were unobtainable. The two peaks above 928nm would have yielded diameters above 1.1nm showing a broader diameter distribution. This would match the distribution found from Raman spectroscopy. These results are equivalent to the diameters known to be produced by the HiPCO synthesis process.

The results concerning the electrical properties are not of the same equivalence. From absorbance spectroscopy only semiconducting CNTs were detected. This is the result of the needed bandgap in order to produce peaks in absorbance spectroscopy. It is however unlikely that the solution did not contain any metallic CNTs. Raman spectroscopy indicated the presence of metallic although the semiconducting were in majority.

Chapter 7

Conclusion

The general purpose with this project is to gain knowledge about the separation of CNTs. The secondary goal of the project is to obtain knowledge about the characterization of CNTs. During the project a number of different techniques have been studied. From the experiments it has been concluded that work on the nanoscale is complicated because direct observation is not possible.

In order to understand the effects which occurs on the nanoscale, a quantum mechanical description is needed. The energy, location, velocity etc. becomes discrete and it is necessary to use the Schrödinger equation. This introduces effects that are used in various experiments such as absorbance, fluorescence and Raman spectroscopy. This is also the case in SEM microscopy where the wave nature of electrons is utilized.

The separation process was done by dissolving CNTs in SDS and D_2O. The dissolving was done by destroying the CNT bundles by shear forces in a mortar, and then sonicating the solution. The SEM pictures showed longitudinal structures of 30-50 nm in diameter. If the CNTs had not been separated these structures would have been larger. The separation of the CNTs can also be indicated from IR spectroscopy because a peak originating from aromatic systems is present in the spectrum. Based on the data from SEM and IR, it can be concluded that the separation was successful.

From the absorbance and Raman spectroscopy experiments the electrical properties of the CNTs can be determined. A value for the ratio between metallic and semiconduction CNTs is obtained. Furthermore the (n, m) values of some CNTs in the solution are obtained. These values are however associated with a large margin error.

Absorbance and Raman spectroscopy can also be used to determine the diameter distribution of the CNTs. By examining the RBM in the Raman spectra the diameter distribution can be approximated. The absorbance peaks correspond to a range of diameters. The peak values are compared to a database in order to find the diameters.

During the P2 project period we have examined and analyzed one of the most

promising structures on the nanoscale, CNTs. Although a complete examination of the CNTs were not possible, due to limitations caused by insufficient time and money, we have achieved an useful understanding about working on the nanoscale.

Chapter 8

Putting into perspective

After a time consuming process using absorbance spectroscopy, fluorescence spectroscopy, Fourier transform infrared spectroscopy, Raman spectroscopy, scanning electron microscopy and atomic force microscopy, it was found that the collected data gave little information about the CNTs. As the main goal of this project, the characterization of the CNTs, was to a certain degree successful but some of the apparatus used to conduct the experiments was not tuned to the purpose. As a result of this some changes would have been relevant if more time and money had been available. If the funding in relation to the equipment used in this project had been of a grater magnitude, then the experiments involving absorbance spectroscopy, fluorescence spectroscopy and atomic force microscopy was to be re-conducted using more sensitive equipment. New experiments involving scanning tunneling microscopy would also be relevant. These experiments could for example have been carried out at low temperatures at around 80 K in order to lower the kinetic energy of the molecular bonds of the CNTs. There by lowering the movement of the individual atom which will result in a much sharper picture. It could also be interesting to use more than one laser in the Raman spectroscopy experiment.

Appendix A

Absorbance Spectroscopy

The principle of absorbtion

Absorbtion of electromagnetic radiation in matter observed in the region of the spectra reaching from uv- over visible- to infrared light must be separated in two. In the case of uv- and visible light the absorbtion happens due to excitations of electrons in the individual carbon atom. In the case of infrared light the absorbtion is due to vibrational excitations of the bonding between atoms. The reason for this difference in the absorbtion is caused by the wavelength of the light. The wavelength of the uv-light is the shortest of the three. This means that the energy of the individual photon is high. The energy makes it possible for the photon to excite the electrons of a atom to a higher quantum state. The energy of visible light is not as high but it can still excite the electrons. Compared to the other wavelength the energy of the infrared light is low. This low energy means that the light can not interact with a single electron in the atom. Instead the light interact with the covalent bonds. The interaction raises the kinetic energy of the bonding in the nanotubes.

The absorbtion spectroscope

The absorbance spectroscopy instrument passes light trough a solution. When the wavelength of the light is changed over time and the different intensities are recorded a spectrum can be drawn. The data collected is an expression of the optical properties of the solution. From the recorded spectrum the excitation wavelength can be found. This is where the peaks occur on the curve. The absorbance can also be calculated using Beer-Lambert's law, se Equation A.1

$$I = I_0 \cdot 10^{\epsilon c l} \tag{A.1}$$

I is the measured intensity, I_0 is the input intensity, l is the path traveled by the light in the sample, c is the concentration and ϵ is the molar absorptivity.

The absorbance A is thereby defined as Equation A.2:

$$A = I_0 \cdot Log_10(I_0/I) = \epsilon cl \tag{A.2}$$

Carbon Nanotubes

In the case of carbon nanotubes it is possible to calculate at which wavelengths excitation will appear. This can be done using Equation A.3.

$$\overline{\nu}_{Abs} = \frac{10^7 cm^{-1} nm}{145.6nm + 575.5 \cdot d} + \frac{A \cdot \cos(3 \cdot \alpha)}{d^2} \tag{A.3}$$

$\overline{\nu}_{Abs}$ is photon frequency in cm^{-1}. A is equal to $1375cm^{-1}nm^2$ for $(n-m)mod3 = 1$ or $-1475cm^{-1}nm^2$ for $(n-m)mod3 = 2$. α is the chiral angle and d is the diameter of the CNT [Bachilo et al., 2002].

Equation A.3 can also be used to characterize which type of nanotube that is analyzed. This is done using the absorbance spectrum, the emission spectrum of fluorescence spectroscopy and the Equation B.1 from Appendix B. The explanation on how this calculation is done can also be found in Appendix B.

Appendix B

Fluorescence

Introduction to Fluorescence Spectroscopy

The history of fluorescence started in 1845 where Sir John Frederick William Herschel described the first observation of fluorescence from a quinine solution in sunlight. Unfortunately Sir John F. W. Herschel did not continue his research into fluorescence and only published a few papers about this subject. Another important person in this context is Alexander Jablonski. Alexander Jablonski was an Ukrainian scientist who completed a remarkable research into the studies of atomic and molecular physic. His work leaded, among other things, to the Jablonski diagram, which explain the processes that occur in fluorescence [Lakowicz, 1999].

The principle of Luminescence

To explain fluorescence it is easy to start explaining luminescence because fluorescence is a part of it. Luminescence is the emission of light from any substance and occurs when electrons are in excited states. Luminescence is divided into two sub categories, fluorescence and phosphorescence, depending on the excited state. In both cases an electron has been excited from a lower energy state to a higher energy state. Afterwards the electron undergoes a radiationless transition to a lower metastable state by emission of heat. From the metastable state the electron returns to the ground state by emission a photon. The energy of the photon is lower than the energy of the photon that excited the electron in the first place, which result in a light with a longer wavelength. A simple form of a Jablonski diagram illustrates these processes in Figure B.1. The difference between fluorescence and phosphorescence is how long time the electron stays in the metastable state. In fluorescence these two transitions take places rapidly. A typical lifetime of fluorescence is about $10ns$. The lifetime of phosphorescence is longer and varies from milliseconds to hours depending on the material. The phenomena of phosphorescence will not further described [Jr. and Owens, 2004].

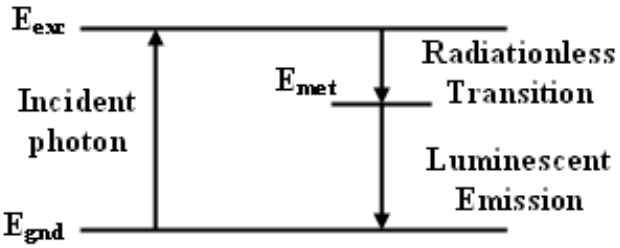

Figure B.1: The process that occurs when an excited electron returns to the ground state under emission of a photon. The radiationless transisition is released as heat.

Spectrofluorometer

To achieve some good results from fluorescence spectroscopy it is necessary to have a good understanding of the equipment. Figure B.2 shows that a spectrofluorometer consist of eight main parts witch are: lamp, dual grating excitation monochromator, optical module, sample chamber, emission monochromator and monochromator controller. This spectrofluorometer has a xenon lamp as the source of exiting light. This type of lamp can produce light with high intensity at all wavelength above 250 nm. The spectrofluorometer shown in Figure B.2 is equipped with monochromators that can select the excitation and emission wavelength. The excitation monochromator contains two gratings, which minimize stray light i.e. light with wavelength different from the chosen wavelength. The optical module contains shutters, filter holder, the beam splitter and polarizers. The shutters can eliminate the exciting light or close of the emission channel. The filter holder contains a bandpass filter, which reduces the intensity of the light from the solution. This reduction is proportional to the intensity of the excitation light. The beam splitter consists of a thin piece of quartz and reflects about 4% of the light to a reference cell. Polarizers are placed in the excitation and emission light paths. Normally the polarizers are removable so that they can be replaced for measurements of fluorescence anisotropy or when it is necessary to select polarized components of the emission and excitation. The sample chamber is where the samples are placed and normally contain a heating element. The monochromator controller collects all the measurements and gives the output data [Lakowicz, 1999].

Carbon Nanotubes

Fluorescence is interesting when dealing with CNTs because the tubes are build of an aromatic system, which normally known to be fluorophores. If diameters and chiral angles for CNTs are known it is possible to calculate where the emission will take place with Equation B.1.

$$\overline{\nu}_{Em} = \frac{10^7 cm^{-1} nm}{157.5nm + 1066.9 \cdot d} + \frac{B \cdot \cos(3 \cdot \alpha)}{d^2} \tag{B.1}$$

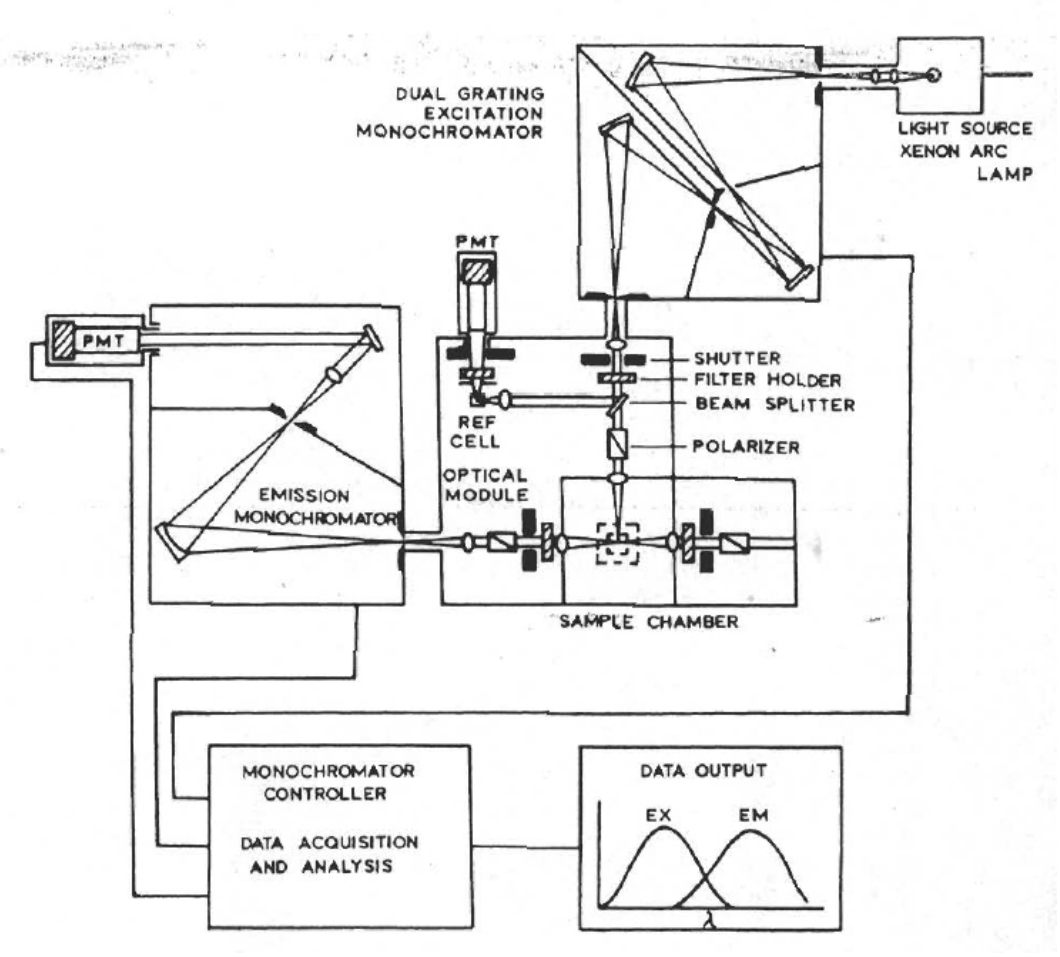

Figure B.2: A sketch of a typical spectrofluorometer. It shows how the light travels through the device. [Lakowicz, 1999]

$\overline{\nu}_{Em}$ is photon frequency in cm^{-1}. B is equal to $-710 cm^{-1}nm^2$ for $(n-m)mod3 = 1$ or $396 cm^{-1}nm^2$ for $(n-m)mod3 = 2$. α is the chiral angle and d is the diameter of the CNT [Bachilo et al., 2002].

Furthermore when the photon frequency for exciting and emission are know for a CNT it is possible to calculate diameter and chiral angle by combining Equation A.3 and Equation B.1.

Appendix C

Fourier Transform Infrared Spectroscopy

Fourier Transform Infrared Spectroscopy

Fourier Transform Infrared Spectroscopy (FTIR) is the preferred method of infrared spectroscopy as this method is faster and more accurate than the other methods of IR spectroscopy.

IR spectroscopy has been used for more than seventy years and it is based on the principles that molecular vibrations occur in the infrared region of the electromagnetic spectrum. This spectrum represents a fingerprint of a sample with absorption peaks which correspond to the frequencies of these molecular vibrations between the atoms of the material. As material consist of different combinations of atoms, the electromagnetic spectrum is unique for each combination. The concentration of a material is shown by the height of the spectrum peaks. [Nicolet, 2001]

IR instruments uses a prism or grating to separate the emitted energy rom the infrared source into individual frequencies. The prism used in infrared light separates the light into frequencies, the same way as the ones used with visible light. The grating separates the infrared light into frequencies same way as a prism but far better. A detector measures the energy for each frequency that has passed though the sample and these results are shown as a spectrum plotted of intensity vs. frequency. This technique takes several minutes as each frequency is measured individually. This is far to long and to overcome this problem, an others, a new method of IR spectroscopy was developed, FTIR. [Nicolet, 2001]

The FTIR spectrometer uses an optical device called interferometer whichproduces a unique type of signal which has all of the infrared frequencies 'encoded' into it. This signal can be measured in just a few seconds. The interferometer consist of a beamsplitter which divides the incoming infrared light into two optical beams. One beam is reflected off a fixed mirror and the other beam is reflected off a movable mirror. The two beams are both reflected back to the beamsplitter and recombined [www.britannica.com, 2005]. As the path to one if the mirrors is fixed and the other

is constantly changing, the signal is the result of the two beams interfering with each other. This signal is called a interferogram and it has the property that the data point which constructs the signal has information about every infrared frequency from the source. The data point are a function of the moving mirror position. As the interferogram is being measured, all frequencies are measured at the same time and therefore this measurement takes seconds instead of minutes. The interferogram can not be interpreted immediately as the analyst needs a plot of intensity at each individual frequency to make an identification. These individual frequencies has to be decoded and this can be done by the mathematical technique, Fourier transformation. The Fourier transformation is made by a computer and the output is the spectrum. [Nicolet, 2001]

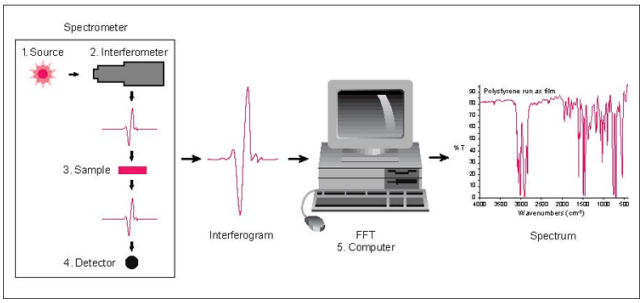

Figure C.1: A simple layout of a FTIR spectrometer. [Nicolet, 2001]

This is also illustrated on Figure C.1 where the infrared energy is emitted from the source and passed though an opening that controls the amount of energy given to the sample. The beam goes into the interferometer where the encoding is done and the interferogram signal is made. The signal is then sent to the sample where is it either transmitted through of reflected off the surface (depending on which method of analysis being used). And here specific frequencies of energy are absorbed. The beam are then sent to the detector which are specially intended to measure the interferogram signal. This measured signal is digitized and finally sent to the computer where the Fourier transformation is performed and the infrared spectrum is presented. A simple layout of a FTIR spectrometer is shown in Figure C.2.

A background spectrum must also be measured as there need to be a relative scale for the absorption intensity. A background measurement is distinctive of the instrument itself and it can be used for many sample comparison. This background spectrum is made by measuring without a sample in the beam and it is used to compare the measurement with a sample to determine the percent transmittance. The result is a spectrum without the instrumental characteristics.

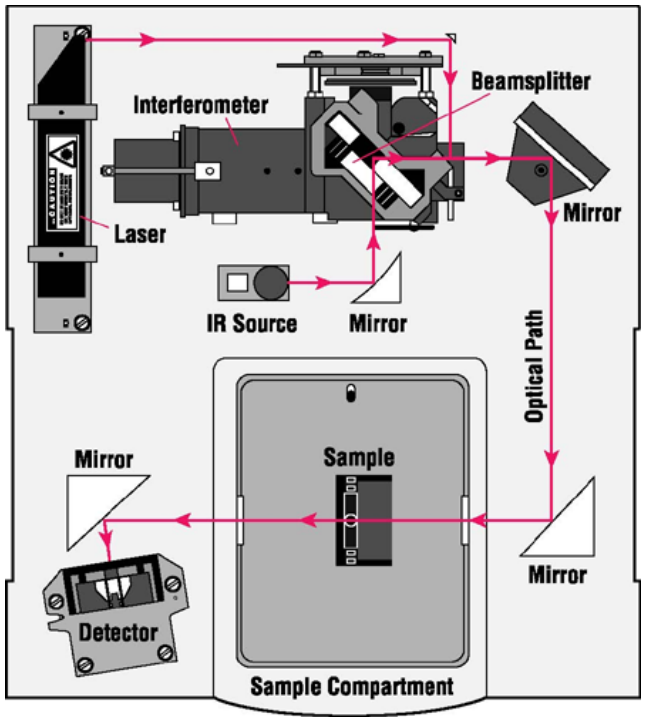

Figure C.2: A layout of a FTIR spectrometer. [Nicolet, 2001]

Appendix D

Raman Spectroscopy

The Raman Effect

Raman spectroscopy is based on the Raman effect which was first discovered by Sir Chandrasekhara Venkata Raman in 1928 [www.britannica.com, 2005]. The Raman effect occurs when an incident beam of light enters matter, and the light is scattered due to collisions between photons and molecules. When the photons hit the molecules of the sample, they causes perturbations of the molecules which induce rotations and vibrational transitions in the molecule. The collisions between photons and molecules can be either elastic or inelastic and the light is scattered dependently. In the case of elastic scattering the light is scattered with no change in wavelength or energy. This type of scattering is called Rayleigh scattering. In the inelastic case the light is scattered with a change in wavelength, and this is called the Raman effect, or Raman scattering. The change in wavelength occurs because the photons can either deliver or gain energy from the molecules in the sample. Energy is transferred from the photons to the molecules by rotational or vibrational transitions. The opposite process is also possible, here energy is transferred to the photons from the molecules and the molecules thereby lose rotation and vibration. This means that Raman scattered light can be of either shorter of longer wavelengths. Scattered light with a longer wavelength is referred to as Raman Stokes scattering, and light with a shorter wavelength is called Raman Anti-Stokes scattering. Only a fraction, approximately 1 of 10^7 photons, of the incident light is scattered by Raman scattering. This makes it difficult to detect the scattered photons and this is the reason why the detector is always positioned orthogonally to the incident light. When the detector is placed in this way, the detected light consists of primarily scattered light, and less of the original light.

Raman Spectrum and Carbon Nanotubes

The Raman spectrum is recorded at a specific excitation wavelength at which the Raman scattering is intense enough to be detected. The Raman spectrum is the

intensity plotted as a function of the scattered wavelengths. Because the Raman spectrum is unique for different matter, it is possible to determine the type of matter in the solution. From the placement of the peaks in the spectrum, different properties of the sample can also be revealed.

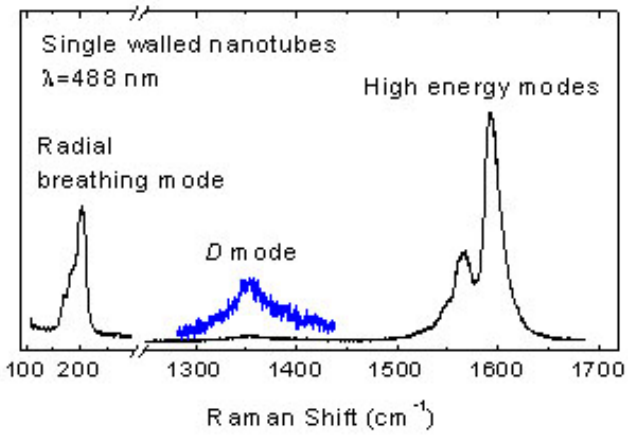

Figure D.1: The placement of the peaks in the raman spectrum of single walled carbon nanotubes [of Cambridge, 2005]

With raman spectroscopy of carbon nanotubes, the placement of the peaks can be used to determine such properties as diameter distribution, metallic character and orientation of isolated tubes. This can be done by examining the position of the radial breathing mode (RBM), disorder induces mode (D-mode) and high energy mode (HEM). The RBM peaks reveals the presence of single walled carbon nanotubes, and these peaks can be used to calculate the diameters through Equation D.1.

$$\omega_R BM = \frac{A}{d_T} + B \tag{D.1}$$

ω_{RBM} is the Raman frequency corresponding to each RBM peak. A and B are arbitrary constants and d_t is the diameter of the tube in nm. For CNT in bundles are A and B equal to $234cm^{-1}nm$ and $10cm^{-1}$ and for isolated CNT are A and B equal to $248cm^{-1}nm$ and 0 [Jorio et al., 2003].

The high energy mode is also refereed to as the G-band and it can reveal the metallic properties of the CNTs. The G-band is a double peak structure, where the left peak normally is labeled G^- and the right peak G^+ [of Cambridge, 2005] These two peaks can be used to predict the conducting or semiconducting properties of isolated CNTs through Equation D.2.

$$\omega_G^- = \omega_G^+ - \frac{\beta}{d_t^2} \tag{D.2}$$

ω_G^- and ω_G^+ are Raman frequency in cm^-1 and β is an arbitrary constant and d_t is the diameter of the nanotube in nm. The arbitrary constant is $47.7cm^{-1}nm^2$ for metallic- and $79.5cm^{-1}nm^2$ for semiconducting CNTs [Dresselhaus et al., 2002].

In cases where a mixture of conducting and semiconducting CNT is analyzed it is not possible to use Equation D.2 because the G^- peak will be a composition of G^- peaks. Instead the difference in intensity between the G^- peak and the G^+ peak can be used to estimate a ratio between conducting and semiconducting CNT. The intensity of the G^- peak is equal the intensity of G^+ peaks for conducting CNT and decrease when the amount of conducting CNT decrease. Therefore the amount of conducting CNT is proportional with the intensity of the G^- peak [Kukovecz et al., 2002].

The D-mode in Raman spectra from graphite represent different defect such as vacancies, heptagon-pentagon pairs, kinks, or the presence of impurities. It is possible that the D-mode represent the same in Raman spectra from CNTs but it have not been proved yet [Dresselhaus et al., 2002].

Appendix E

Atomic Force Microscopy

Atomic Force Microscope

Atomic force microscope is one of the most popular and useful scanning probe microscopes. It operates on simple principles to gain data about the differences in height in the surface of a sample.

The Birth of Atomic Force Microscope

One of the biggest disadvantages of STM is that it can only be used on conductive samples. If the sample is nonconductive there can be no electron tunneling between the tip and the sample, when a voltage is applied between them. Soon after the STM was invented, it was clear that another type of SPM, which allowed for nonconductive samples, was needed. This resulted in the AFM which was developed 5 years after the introduction of STM [Birdi, 2003].

Principles of Atomic Force Microscope

AFM is based on much of the same principles as STM except that AFM does not use the tunneling effect to measure surface topography; instead it uses forces between the tip and the sample. When the tip is exposed to forces, it causes the cantilever to bend and this bending can be measured and processed to create a topographical image of the surface. Several forces typically contribute to this bending of the cantilever. The force which is most often associated with AFM is the Van Der Waals forces. Van Der Waals forces is an attractive force. When the tip to sample seperation approaches zero, the repulsive force is caused by a combination of columb forces and overlapping electron clouds. Figure E.1 shows the force as a function of distance.

The curve clearly shows the regions in which the force is repulsive and those in which it is attractive. AFM operates in both the contact region, which is often called Direct Contact AFM or DC-AFM, and the non-contact region also called NC-AFM.

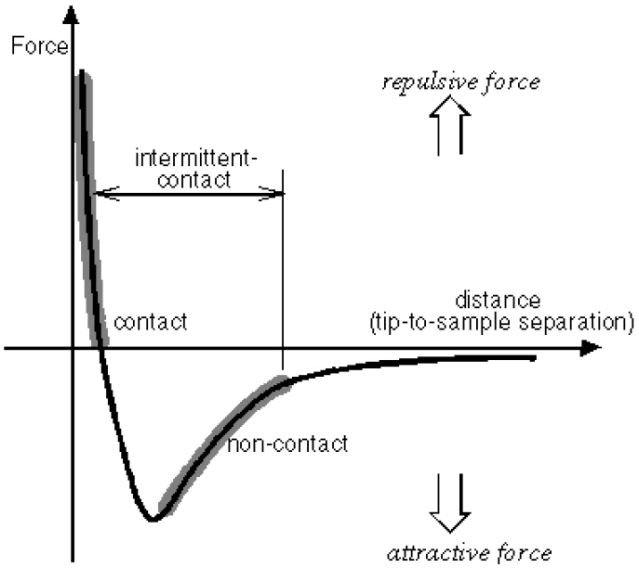

Figure E.1: This picture shows the relationship between force and distance. In the left side of the diagram the force is repulsive caused by columb forces and overlapping electron clouds. In the right side the force is attractive caused by van der Waals forces.

Another mode of AFM operates in the intermittent-contact region, and this is called IC-AFM. Which mode is preferred depends on the situation as will be described in the following sections. One of the main advantages of the AFM technique is the power of magnification and resolution. While optical microscopy is limited by the wavelength of visible light, the AFM is not. The resolution of an AFM is determined by the size of the tip, the step length and the step size of the image. The AFM instrument accessible, has an resolution of 15 nm. With STM atomic resolution is possible.

Contact AFM

In this mode of AFM, the tip is situated in the contact region shown on Figure E.1. The principle in this mode of operation can largely be compared to the old record player, where a sharp metal needle moved on top of a vinyl record to reproduce sound [Birdi, 2003]. The vertical movement of the metal needle directly translated to sound, in DC-AFM the deflection of the cantilever directly translates into a topographic image of the surface. The deflection of the cantilever is due to overlapping electron clouds, and the columb forces which are experienced in the contact region. When the atoms of the tip and the sample are brought close together, below 1 nm [Howland and Benatar, 2000], the electron clouds of the tip and sample atoms repel each other, and thereby cause the cantilever to bend. The magnitude of the deflection is determined by the cantilever spring constant, and generally has to be lower

than the spring constant between atoms in the sample which is in the order 10 N/m [Howland and Benatar, 2000]. If the spring constant of the cantilever is larger than that of the atoms in the sample, a deformation of the sample might occur.

Detection of the cantilever deflection is done with the help of a position sensitive photo detector or PSPD for short. A laser beam is focused at the cantilever and the reflection reflects the deflection of the cantilever as shown in Figure E.2.

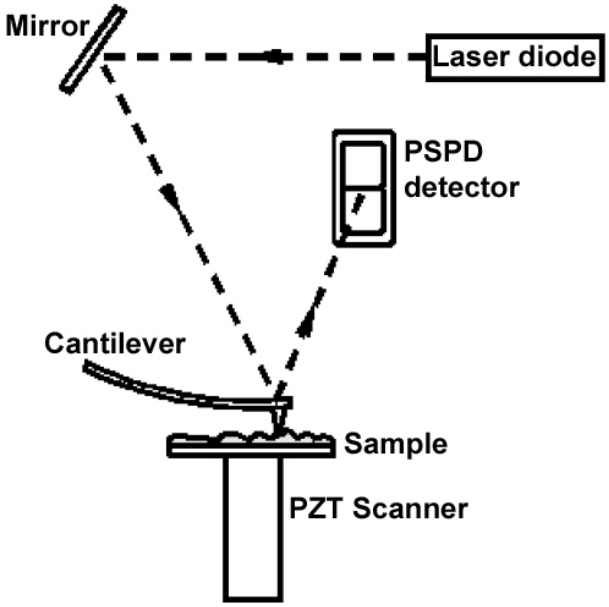

Figure E.2: The PSPD device. The light is being reflected from the cantilever and the deflection of the cantilever can be detected. The longer the distance from the cantilever to the PSPD device, the larger angle.

When a deflection is registered by the PSPD, two modes of operation is of choice. The AFM can either be operating at constant force or constant height mode. In constant force mode the deflection causes a feedback system to adjust the height of the cantilever, keeping the force constant. As soon as the force increases the height of the cantilever is increased as well, to keep the force constant. In constant height mode, the height of the cantilever is kept constant and the deflection of the cantilever varies with the surface topography. In constant force mode, it is the up and down movement of the cantilever which produces the image, whereas in constant height mode, it is the deflection which directly produces the image.

Non-Contact AFM

This mode of AFM differs from DC-AFM in that it operates in the non contact section seen on Figure E.1. The driving force in the non-contact region is the

Van der Waals force. Where DC-AFM has the probe situated at a distance below 1 nm from the sample, NC-AFM has the probe at a distance of 10 to 100 Å from the sample [Howland and Benatar, 2000]. The cantilever is vibrated near its resonant frequency with an amplitude of 10-100 Å using a piezo electric device [Howland and Benatar, 2000]. This vibration is disturbed when the tip approaches the sample, and this can be used to measure the topography of the surface. When the system detects a change in amplitude, it moves the cantilever up or down to keep amplitude constant. This up/down movement can be used to create an image of the surface, in the same way as with constant force DC-AFM.

Appendix F

Scanning Electron Microscopy

In 1923 the French physicist Louise de Broglie postulated that because photons have both wave and particle characteristics, perhaps all forms of matter have both these properties. At this time it was only a postulate but later it was experimentally proved that electrons have a wave nature. Louise de Broglie was awarded the Nobel Prize in 1929 for this prediction [Serway and Jewett, 2004].

The discovery of the dualism of electrons lead to the idea of using electrons instead of photons in a microscope, and in 1931 the two German physicists Max Knott and Ernst Ruska designed the first electron microscope [www.unl.edu, 2005]. Today several types of electron microscopes exist, and the most often used is the transmission electron microscope (TEM) and scanning electron microscope (SEM) [Serway and Jewett, 2004]. TEM is not used in this rapport and therefore it will not be described any further.

An electron microscope is in many respects similar to an optical microscope. Instead of using a visible light beam to illuminate the object, an electron beam is used. The use of electrons make it possible to obtain a greater magnification because of the shorter wavelength of electrons. The reason for the shorter wavelengths is the energy of the electrons. Electron can gain more energy than the energy of photons. An optical microscope is capable of magnifying an object up to $2,000 times$ but a SEM is capable to magnify an object more than $100,000$ times, depending on the amount of energy being sent though the sample. [www.britannica.com, 2005]. In Figure F.1 a SEM picture of a SWNT is depicted. The de Broglie wavelength of an electron can be calculated with equation Equation F.1,

$$\lambda = \frac{h \cdot c}{E} \tag{F.1}$$

Where λ is the wavelength, h is Planck's constant, c is the speed of light and E is the Energy of the electron.

To create an electron beam an electron gun is used, see Figure F.2. Firstly a positive electrical potential is applied to the anode and a negative electrical potential is applied to the Whenelt Cap. The filament (cathode) is heated until a steam of electrons is produced. The positive potential from the anode accelerates the electron

down the column. The negative potential from the Whenelt Cap repel all angled electrons toward the optic axis. In the space between the filament tip and the Whenelt Cap a collection of electrons occurs, and this is called the space charge. The electrons in the bottom of the space charge exit the Whenelt Cap and can be used to illuminate an object. The electrons, which leave the gun, will be monochromatic and almost parallel to the optic axis [www.unl.edu, 2005].

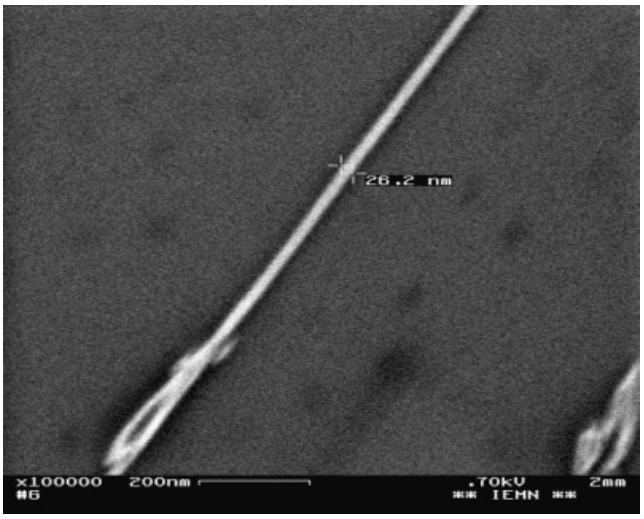

Figure F.1: Shows a 100.000x magnified picture of a SWNT coated by SDS[Dresselhaus et al., 2001]

This electron beam is sent towards the sample, where it interacts with the sample and as it is illustrated in Figure F.3 a number of interactions occur. Depending on what kind of electron microscope is used to examine the sample, different interactions are utilized. SEM utilizes those electrons that are reflected by the sample when the electron beam hits the sample. Backscattered electrons are caused by electrons colliding with atoms in the sample and the scattered backward 180 degrees. The production of backscattered electrons depends on the atoms in the sample. Atoms with a high atomic number produce more backscattered electrons compared with lower numbered atoms. The difference in production of backscattered electron can be utilized to differentiate parts of the sample that have different atomic numbers. Secondary electrons occur when an incident electron passing an atom in the sample close enough to some of the energy from the electron is imparted to a lower energy electron in the atom. This interaction causes a path change of the incident electron. The ionized electron leaves the atom as a secondary electron. The low energy of the secondary electron causes that only those closer than 10 nm to the surface can exit the sample. By counting the secondary electron, which leaves the sample it is possible to get a topographical picture of the sample. To avoid any interactions before the electron beam hits the sample SEM examinations are performed in vacuum [www.unl.edu, 2005].

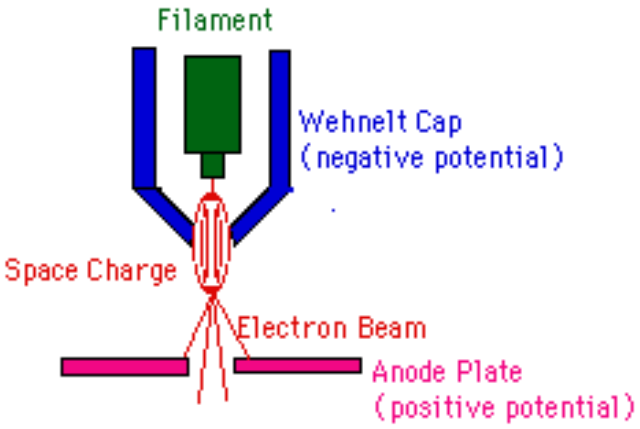

Figure F.2: A model of an electron gun [www.unl.edu, 2005]

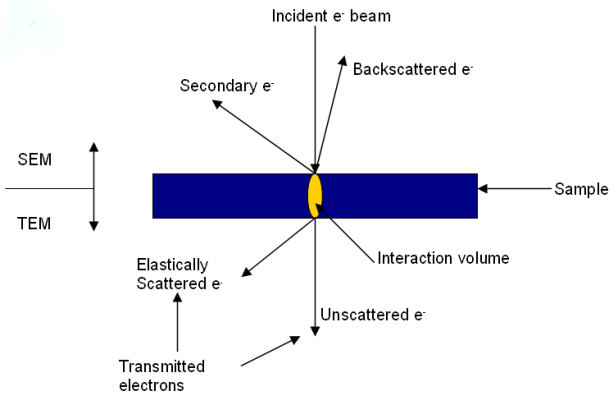

Figure F.3: Those interactions, which is utilized in transmission electron microscope and scanning electron microscope. Modified from [www.unl.edu, 2005]

In Figure F.4 a SEM is sketched. In the top is the virtual source (electron gun), which produces a steam of monochromatic electrons. Below the virtual source the first condenser lens and the condenser aperture are placed. These two components are used to form the steam and to eliminate those electrons, which have an angle to far from the optic axis. The second condenser lens forms the electrons into a thin tight coherent beam. Under the second condenser lens is an objective aperture placed to eliminate high-angle electrons that can have been created by the second condenser lens. After the objective aperture the beam pass through a set of coils. These coils can change the direction of the beam and thereby make the beam scan over the sample. Before the beam hits the sample it passes though an objective lens, which focuses the scanning beam. When the beam hits the sample interactions occur inside the sample and the yield of backscattered and secondary electron are detected before the beam moves to the next point on the sample. The backscattered electrons

are detected by a detector, which is placed under the scan coils. To measure the yield of secondary electrons, they have to be leaded to the secondary electron detector, which is done by a collector. A collector is a grid or mesh with a +100V potential applied to it, which is placed in front of the detector. The collector attracts the secondary electrons to it, which then pass through the holes in the grid or mesh into the detector. A computer uses the detected yields of backscattered and secondary electrons to create a picture of the sample [www.unl.edu, 2005].

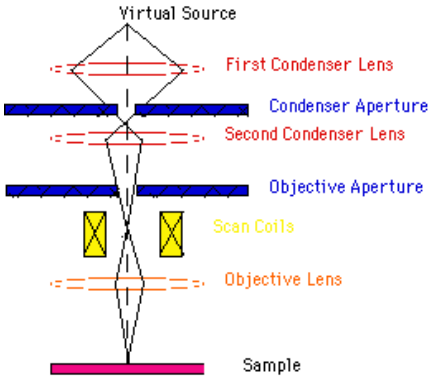

Figure F.4: Sketch of a scanning electron microscope

Bibliography

[Bachilo et al., 2002] Bachilo, S., Strano, M., Kittrell, C., Hauge, R., Smalley, R., and Weismann, R. (2002). Structure-assigned optical spectra of single-walled carbon nanotubes. *Science Magazine*.

[Birdi, 2003] Birdi, K. S. (2003). *Scanning Probe Microscopes: Applications in Science and Technology*. CRC Press.

[Brier, 1994] Brier, S. (1994). *Verdensformlen der blev væk*. Aalborg Universitetsforlag.

[Cyrille, 2005] Cyrille, R. (2005). Supramolecular self-assembly of lipid derivatives on carbon nanotubes. *Science Magazine*.

[Dresselhaus et al., 2002] Dresselhaus, M., Jorio, A., Filho, A. S., Dresselhaus, G., and Saito, R. (2002). Raman spectroscopy on one isolated carbon nanotube. *Science Magazine*.

[Dresselhaus et al., 2001] Dresselhaus, M. S., Dresselhaus, G., and Avouris, P. (2001). *Carbon Nanotubes, Synthesis, Structure, Properties and Applications*. Springer.

[Dumé, 2005] Dumé, B. (2005). Nanobulbs make their debut. Published on the World Wide Web. `http://nanotechweb.org/articles/news/3/6/3/1`.

[Føllesdal et al., 1995] Føllesdal, D., Walløe, L., and Elster, J. (1995). *Politikens introduktion til moderne filosofi og videnskabteori*. Politiken.

[Goddard, 2003] Goddard, W. A. (2003). *Handbook of nanoscience, engineering, and technology*. CRC Press.

[Harris, 1999] Harris, P. J. F. (1999). *Carbon Nanotubes and related structures*. Cambridge University Press.

[Howland and Benatar, 2000] Howland, R. and Benatar, L. (2000). *A Practical Guide to Scanning Probe Microscopy*. ThermoMicroscopes.

[Jorio et al., 2003] Jorio, A., Pimenta, M. A., Filho, A. G. S., Saito, R., Dresselhaus, G., and Dresselhaus, M. S. (2003). Characterizing carbon nanotube samples with resonance raman scattering. *New Journal of Physics*.

[Jr. and Owens, 2004] Jr., C. P. P. and Owens, F. J. (2004). *Introduction to Nanotechnology*. John Wiley and Sons.

[Kittel, 2005] Kittel, C. (2005). *Introduction to Solid State Physics*. Wiley.

[Kukovecz et al., 2002] Kukovecz, A., Kramberger, C., Georgakilas, V., Prato, M., and Kuzmany, H. (2002). A detailed raman study on thin single-wall carbon nanotubes prepared by the hipco process. *European physical journal*.

[Lakowicz, 1999] Lakowicz, J. R. (1999). *Principles of Fluorescence Spectroscopy*. Plenum US.

[leksikon.org, 2004] leksikon.org (2004). Naturvidenskab. `http://www.leksikon.org/art.php?n=1832`.

[mhhe.com, 2005] mhhe.com (2005). Orbital shapes. `http://www.mhhe.com/physsci/chemistry/essentialchemistry/flash/hybrv18.swf`.

[Nantero, 2005] Nantero (2005). Nram. `www.nantero.com`.

[Nicolet, 2001] Nicolet (2001). *Introduction to Fourier Transform Infrared Spectrometry*. Termo Nicolet Corporation.

[Nikolaev et al., 2004] Nikolaev, P., Bronikowski, M. J., Bradley, R. K., Rohmund, F., Colbert, D. T., Smith, K., and Smalley, R. E. (2004). Gas-phase catalytic growth of swnt from carbon monoxide. *Science Direct*.

[O'Connell et al., 2002] O'Connell, M. J., Bachilo, S., Huffman, C. B., Moore, V. C., Strano, M. S., Haroz, E. H., Rialon, K. L., Boul, P. J., Noon, W. H., Kittrell, C., Ma, J., Hauge, R. H., Weisman, R. B., and Smalley, R. E. (2002). Band gap fluorescense from individual single-walled carbon nanotubes. *Science Magazine*.

[of Cambridge, 2005] of Cambridge, U. (2005). Raman scattering on carbon nanotubes. Published on the World Wide Web. `http://www-g.eng.cam.ac.uk/edm/research/nanotubes/CNT_raman.html`.

[Serway and Jewett, 2004] Serway and Jewett (2004). *Physics for Scientists and Engineers*. Thomson.

[SME, 2004] SME (2004). Forelæsning, studiets metoder.

[Stix, 2005] Stix, G. (2005). Nanotubes in the clean room. *Scientific America*.

[uni potsdam.de, 2005] uni potsdam.de (2005). wizard. `http://www.chem.uni-potsdam.de/cgi-bin/irwiz2.pl`.

[wikipedia.org, 2005] wikipedia.org (2005). Wikipedia. `http://en.wikipedia.org`.

[writing.colostate.edu, 2004] writing.colostate.edu (2004). Validity. `http://writing.colostate.edu/references/research/relval/`.

[www.britannica.com, 2005] www.britannica.com (April 13th, 2005). Britannica. http://search.eb.com/eb/article?tocId=80602.

[www.iljinnanotech.co.kr, 2005] www.iljinnanotech.co.kr (April 24th, 2005). Iljin nanotech. http://www.iljinnanotech.co.kr/en/home.html.

[www.ing.dk, 2005] www.ing.dk (March 15th, 2005). Ingenioren. http://www.ing.dk/article/19960823/INFOMEDIAARKIV/608230360\&SearchID=73202074629765.

[www.unl.edu, 2005] www.unl.edu (Marts 7th, 2005). University of nebraska lincoln. Published on the World Wide Web. http://www.unl.edu/CMRAcfem/em.htm.

[Zumdahl and Zumdahl, 2003] Zumdahl, S. S. and Zumdahl, S. A. (2003). *Chemistry*. Houghton Mifflin.